Order Number 1349484

Analysis of rock fragmentation using digital image processing

Devgan, Ashutosh, M.S.

The University of Arizona, 1992

U·M·I

300 N. Zeeb Rd.
Ann Arbor, MI 48106

ANALYSIS OF ROCK FRAGMENTATION USING DIGITAL IMAGE PROCESSING

by

Ashutosh Devgan

A Thesis Submitted to the Faculty of the

DEPARTMENT OF MINING AND GEOLOGICAL ENGINEERING

In Partial Fulfillment of the Requirements
For the Degree of

MASTER OF SCIENCE
WITH A MAJOR IN MINING ENGINEERING

In the Graduate College

THE UNIVERSITY OF ARIZONA

1 9 9 2

STATEMENT BY AUTHOR

This thesis has been submitted in partial fulfillment of requirements for an advanced degree at the University of Arizona and is deposited in the University Library to be made available to borrowers under rules of the Library.

Brief quotations from this thesis are allowable without special permission, provided that accurate acknowledgment of source is made. Requests for permission for extended quotation from or reproduction of this manuscript in whole or in part may be granted by the head of the major department or the Dean of the Graduate College when in his or her judgment the proposed use of the material is in the interests of scholarship. In all other instances, however, permission must be obtained from the author.

SIGNED: 

APPROVAL BY THESIS DIRECTOR

This thesis has been approved on the date shown below:

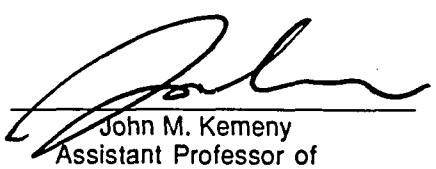

John M. Kemeny
Assistant Professor of
Mining Engineering

7/30/92
Date

ACKNOWLEDGEMENTS

I would like to thank Dr. John Kemeny for his guidance and advice in preparing this thesis. I am especially grateful for the time he spent in the discussion of thesis topics as well as in the evaluation and correction of this thesis.

I would also like to express my appreciation to Dr. Y. C. Kim and Dr. Satya Harpalani for being my committee members and reviewing the manuscript. Their comments and suggestions were very precious. I wish to thank Cyprus Minerals Corporation, US Forest Service, and Department of Interior for funding this research which enabled me to carry out this work. I would also like to thank Roberta Hagaman for her help in the statistical analysis.

I'm deeply indebted to my parents and Bobby. Without their love and encouragement, I could never have reached my goal of higher education.

TABLE OF CONTENTS

LIST OF ILLUSTRATIONS

LIST OF ILLUSTRATIONS-- Continued

LIST OF TABLES

ABSTRACT

The success of rock fragmentation due to blasting depends on many variables, such as rock properties, in-situ fracturing, and blast design. Traditionally, the size distribution of fragmented rock particles has been determined through screen sieving. Modern techniques using video images and computer image processing techniques have the potential for analyzing rock fragmentation accurately and efficiently.

A procedure has been developed for analyzing rock fragmentation which uses a high-resolution video camera for capturing images in the field, and specialized computer algorithms for processing these images. First of all, computer algorithms have been developed to delineate the individual rock fragments in the images. Secondly, a set of experiments have been conducted in the laboratory, in which the two dimensional information from the images is correlated with sieve results. Based on these experiments, a set of probabilities have been determined for correctly determining the size and volume of rock fragments from two dimensional images. Using these probabilities along with the particle delineation algorithm, the size distribution for the rock fragments is calculated. The computer algorithms can also combine information from many images to take into account sampling and images taken at different scales.

CHAPTER 1

INTRODUCTION

The measurement of fragmentation, or the size distribution of blocks resulting from rock blasting, has always been of interest to the mining industry. For the purpose of optimizing blasting operations, attempts have been made to evaluate and predict the size distribution of the fragments in a blasted muck pile. Consequently, operators and others have used visual observations of blasted rock piles to assess the effectiveness of the blasting practice used. It presents one of the most challenging questions in contemporary dynamic rock mechanics. There have been attempts to solve this problem by several techniques. These range from sieving in small scale blasts, or by means of empirical formulae and computer simulations, as well as photographic methods.

The breakage of rock by explosives forms an important though not entirely understood aspect of the mining process. In order to effectively control and optimize the process it is essential that a rapid and reliable technique for assessing the blast results be evolved. Photographic techniques have been developed involving the measurement of some parameter of the block size, e.g. cross-sectional area, diameter or length. Both 35mm photography and on-line video images have been used to record blast fragmentation results. Subsequent analysis methods utilize either manual digitizing or automatic image capture and computer processing.

The effectiveness of blasting can be estimated by determining the size distribution of the blasted rock fragments. The size distribution is usually presented on a plot of percent passing versus size, where the size usually refers to the screen size. There are many methods to estimate the size distribution of blasted rocks. The most direct method is to sieve the blasted rocks through screens with different mesh sizes

(Clark, 1987). The high cost of sieving for tons of blasted material has led to many indirect methods for estimating the size distribution. One of the more recent and popular methods is photoanalysis, where photographic images are obtained from the surface of a pile of blasted rocks and analyzed either by hand or through computer image processing techniques (Franklin et al., 1988; Ghosh et al., 1990; Mojtabai et al., 1989).

Many problems are encountered when trying to estimate fragmentation using photographic images. First of all, the individual rock fragments in the image must be delineated, either by hand or using image processing techniques. Problems with non-uniform lighting, shadows, noise, and the great range in fragment sizes make delineation virtually impossible using standard edge-detection routines. A second problem is correctly extracting three-dimensional information from the two-dimensional images. Assumptions about the fragment sizes in the third dimension need to be made. Also, rock fragments will overlap, and corrections on the fragment sizes due to overlap need to be made. Finally, assumptions need to be made about the relationship between the size distribution on the surface of a pile, and the overall size distribution in the three-dimensional volume.

We propose a new procedure for calculating the size distribution of rock fragments using digital image processing. For new procedures to be widely accepted and applied, they must be verified as to their accuracy, ease of use, and reproducibility, as well as reproduce results found using former methods. Realistically, new methods will replace old methods only if they represent an improvement in the old method or require less time, effort, or a smaller sample size, or if they are more accurate (Frankenburg, 1990).

The procedure that we have developed for analyzing rock fragmentation uses a high-resolution video camera for capturing images in the field, and specialized computer

algorithms for processing these images. An algorithm for delineating the individual rock fragments automatically has been developed (Kemeny and Wu, 1992). The algorithm is based on the shadow regions that fill void spaces and partially occur along fragment edges. Using this algorithm, the rock fragments are delineated. Also, experiments have been conducted in the laboratory, comparing the size distribution from images taken at the surface of rock piles with sieving of the piles. Based on these experiments, a set of probabilities have been determined for correctly determining the size of rock fragments from two dimensional images. Using these probabilities along with the particle delineation algorithm, the size distribution of rock fragments is calculated. The procedure is fully automated, runs quickly and is accurate. Results obtained by this procedure have been compared to the sieve results and have been found to be satisfactory.

CHAPTER 2

BACKGROUND

The aim of a mining or quarry operation is to produce rock fragments of some optimum size and shape as effectively and economically as possible. In heap leaching of copper oxides, for instance, blasting is the only size reduction that occurs prior to leaching. A correlation exists between the size of the fragments in the leach pile and the percentage of copper that can be recovered, making it important to optimize the fragmentation from blasting. A secondary aim is to improve and reduce the number of processes such as blasting and crushing involved in producing these rock fragments. In order to accomplish both aims, it would be useful to know the size and shapes of the fragments before and/or after each process (Ord, 1989). The success of rock fragmentation due to blasting depends on many factors, such as rock properties, blast design and in-situ fracturing (Farmer et al., 1991).

The ideal design of a blast should produce a fragmentation closely matched to that required for a specific application, and reduce to a minimum the need for secondary blasting and crushing. Improved fragmentation in most applications means smaller blocks, and generally requires more drilling and more explosives. The costs, however, are offset by easier and cheaper loading , hauling, and crushing (MacKenzie, 1966; Greenland and Knowles, 1969). The size of the fragments and their distribution in the broken material produced by blasting can be classified by the size of the blast, the explosive distribution, the in-situ structure of the rock, and the structure of the blast, including geometry, explosive distribution, and confinement (Clark, 1987).

The mining industry could profit from a fast and accurate method for determining the fragment size distribution before and after blasting. In certain rock conditions, say

in very weak or strong areas of a mine, the pattern of blasting may be inefficient. Differences in block size distribution by as much as 20% can be difficult to detect from visual comparisons of blasts. Traditionally, the size distribution of fragmented rock particles has been determined through screen sieving. Computer analysis could improve the efficiency of rock fragmentation. Modern techniques of calculating the size distribution use video images and computer image processing techniques (Farmer et al., 1991). Manual digitization of photographs of muck heaps has been described by MacLachlan and Scoble (1986), Sheokh and Chung (1987), and Maerz et al (1987). Predictions have also been made from blasting parameters and rock mass properties, either using empirical formulae (Lovely, 1973; Just and Henderson, 1971), or from computer simulations (Gamma, 1984).

However, all of the above techniques have difficulties. Sieving has been used extensively in scaled down blasting tests (Dick et al., 1973; Bhandari and Vutukuri, 1974; Singh et al., 1980), and is still used in mining and quarrying situations, including research, for determining size and shape distribution. But it is a time consuming process, and is very expensive for the treatment of large volumes of material (Ord, 1989).

Several mathematical models for different types of fragmentation and comminution have been proposed to represent the relationship of the particle size distributions that result from drilling and blasting processes, from mechanical comminution and from other fragmentation operations. However, though some of these models apply to the data and describe the products for given blasting operations done under experimental or other specific conditions, they may not apply to the results of tests performed under different conditions. No model appears to fit data from both explosive and mechanical processes or from both small-scale and large-scale operations. Some of the models include factors to describe the explosive quantity and

configuration but appear to have application only where local conditions can be accounted for fitting the data to a given model (Clark, 1987). Photographic methods have been developed in which some parameter of block size, such as length or cross sectional area, is measured on the image either manually (Carter, 1977; Aimone and Dowding, 1983; Noren and Porter, 1974) or using an image analyzing computer (Gozon, 1986). Problems with determining the size distribution with photographic methods include sampling, image resolution, noise, and interpreting three-dimensional information from two-dimensional photos. These are discussed in detail in later chapters.

2.1 Digital Image Processing

Digital image processing came into existence because of a need for transferring images from one place to another quickly and with a minimal loss in image quality. In addition to applications in the space program, digital image processing techniques are used today in a variety of problems which, although often unrelated, share a common need for methods capable of enhancing pictorial information for human interpretation and analysis. Image enhancement and restoration procedures have been used to process degraded images depicting unrecoverable objects or experimental results too expensive to duplicate. A digital image is an image which has been discretized both in spatial coordinates and in brightness. We may consider a digital image a matrix whose row and column indices identify a point in the image and the corresponding matrix element value identifies the gray level at that point. The elements of such a digital array are called picture elements, or pixels (Gonzalez and Wintz, 1987).

Digital image processing involves digitizing an image on the computer, and filtering and processing the image in order to highlight the desired objects or calculate various quantities (Gonzalez and Wintz, 1987; Young and Fu, 1986). The image is broken down into pixels, and arranged in a two dimensional matrix. In an 8-bit image,

Figure 2.1 : An example of a 256 gray scale image.

each pixel represents the intensity of light at that point to one of 256 discrete intensity levels, which is otherwise known as a 256 gray level scale (Ord, 1989). Although the size of a digital image varies with the application, a typical size comparable in quality to a monochrome TV image is a 512 x 512 array with 128 gray levels (Gonzalez and Wintz, 1987).

The image shown in Figure 2.1 consists of a 346 x 248 array of pixels with 256 gray levels. This closely simulates a photograph. For this study a 640 x 480 array of pixels was the maximum size of image used. The size of such an image is about 300 Kb. The processing is either done on the pixels and their associated gray levels, or with the frequency spectrum of the image (via Fourier or other transforms). For instance, edges in a digital image can be enhanced by weighing the high frequency components of the transformed image (and then taking the inverse transform). Another technique of image processing is to assign colors to different ranges of gray level or frequency. Shadows and noise can be removed from the images by using various filters (Farmer et al., 1991).

The gradient value for a pixel is a measure of the contrast in gray level between the pixel and neighboring pixels. A high gradient value may indicate the presence of a boundary of a fragment. Many standard procedures exist for calculating the gradient value for each pixel in a digital image (Gonzales and Wintz, 1987). The gradient alone is not a good indicator for fragment edges, since noise will also give high gradient values. Noise in a digital image can be due to a number of features. For the purposes described in this thesis, noise consists of the following features. 1. Color changes in the rock. 2. Certain surface features like surface roughness, surface irregularities, and texture. 3. Irregular contact between two rock particles. This includes shadows, packing arrangement, or the nature of contact. 4. Non-rock features such as rulers, vegetation, soil, water, etc.

2.2 Particle Delineation

One of the major problems with using digital image processing for analyzing fragmentation is first teaching the computer to identify the individual fragments in an image. The computer needs to differentiate between fragment edges and various types of noise such as surface roughness, shadows, and color differences. The computer must also completely outline each of the fragments. Edge detection filters are often used for this purpose. However, the edge detection filters developed so far have not been able to solve the problem of delineation completely. A method of particle delineation has been developed that does not rely on edge detection filters, as discussed in section 3.3. Once the particles have been delineated, the 256 gray level image is reduced to a binary image(all pixels have value either 255 or 0, Figure 2.2 is an example of the binary image) where the fragments are white and the background is black (or vice versa). Figure 2.2 is the binary file of Figure 2.1 after it has been delineated by algorithms described in section 3.3.

2.3 Image Capture

There are many ways in which the images can be captured in the computer. The two most common methods involve either scanning photographs with a gray scale scanner, or capturing frames from a video camera using an image capture board in the computer. A high resolution video camera (approximately 400 TV lines) gives a significant improvement in resolution compared with the standard video camera (approximately 260 TV lines). If the tape medium on the video camera is an 8mm tape, the high resolution camera is referred to as a "High-8" camera. If the tape medium is a VHS tape, then the high resolution camera is referred to as a "Super-VHS" or "S-VHS" camera.

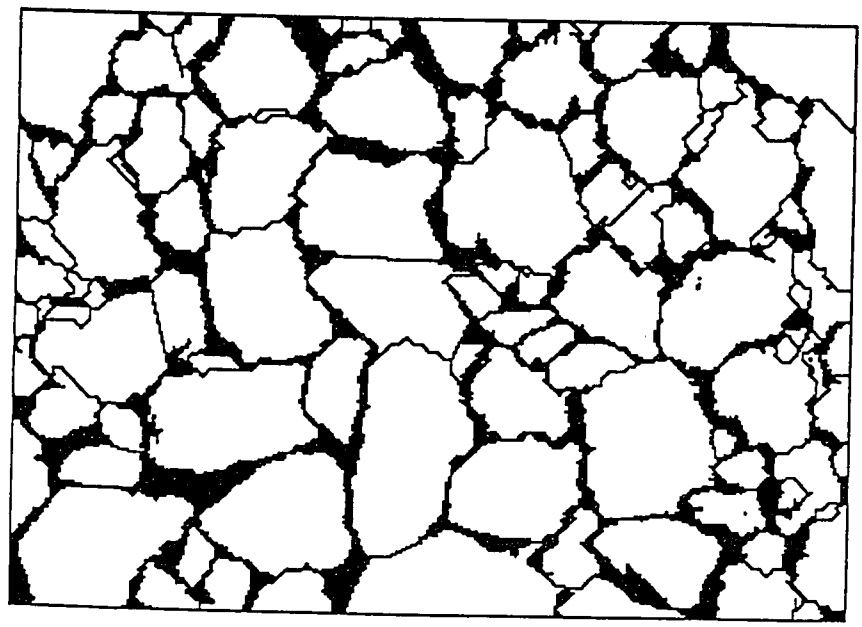

Figure 2.2 : Binary file of Figure 2.1. The particles have been delineated by using the algorithms described in section 3.3.

2.4 Problems with Fragmentation Analysis Using Digital Image Processing

Some of the problems associated with analyzing digital images on the computer include accurately delineating each of the rock fragments, eliminating noise, and correctly characterizing the three dimensional statistical distribution of the fragments from two dimensional images. These topics will be discussed below.

Fragmentation analysis using photoanalysis has been criticized in the past for a bias in sampling. The muck pile is clearly heterogeneous with respect to fragment size. The largest sizes appear to have a tendency to be thrown to the forward fringes of the pile, and the smallest to cover the upper surface. Sizes appear to increase progressively from the back to the front of the pile, and lateral variations are also possible. The shape and position of the particles in the muck pile also effects the analysis. A particle may be close to cylindrical in shape and may have a very long third dimension, but due to its position in the muck pile, it may appear that its third dimension is much smaller. Another case may be that a large particle with a very small third dimension may look much smaller if it has been covered by other particles in the pile. The reverse is also true. A particle with one of the dimensions small, may appear larger in the pile. For elongated fragments, the long axis of the fragments can be significantly larger than the screen sizes that the fragments passed through. What determines the minimum screen size for a fragment are the minimum and intermediate dimensions. The way a particle lands in a muck pile and the position it finally occupies is governed by its size, shape, velocity and other blast design factors.

Once the individual fragments in an image have been delineated, various quantities can be calculated for each fragment, such as perimeter, area, orientation, and the major and minor axes of an equivalent ellipse fit through each rock particle. The block size distribution is a plot of the percent of the total volume less than a given sieve

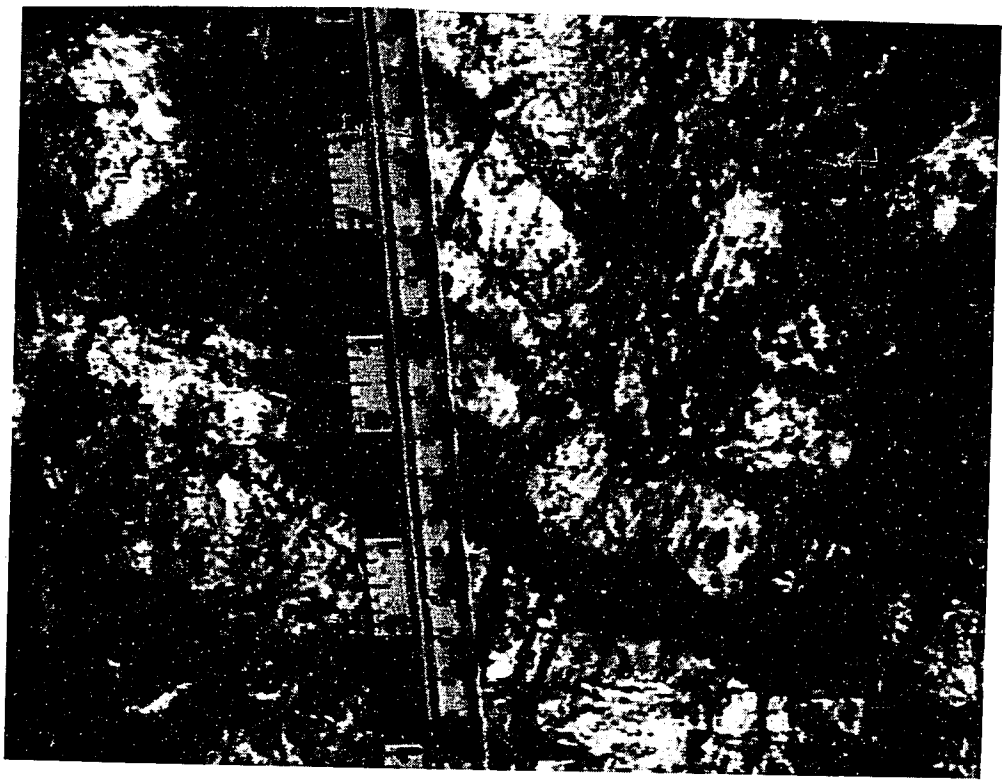

Figure 2.3 : Example of the intact rock treated with water to enhance the fractures.

size (also referred to as % less than) vs. block size. In order to calculate the block size distribution curve, both the sieve size and the fragment volume have to be estimated from the image parameters. Corrections must be made for fragment overlap and other factors. Also, many images must be analyzed to take into account sampling and scale. Because of all these factors, the difficulty of accurately calculating the size distribution from a two dimensional photograph can be appreciated.

2.5 Effects of In-situ Fracturing

Recent studies have indicated that in-situ fracturing plays an important role in rock fragmentation by blasting. Attempts have been made to determine the block size distribution before blasting by studying the fractures on the face before the blast. Capturing all the fractures on the video camera and then processing them by image processing is a tedious process, and does not always produce satisfactory results. Procedures are now being developed to delineate fractures in images of rock faces in much the same way as the individual fragments are delineated using edge-detection filters or other methods. For these procedures it is advantageous to treat the face prior to imaging in order to highlight the fractures. Spraying water on the face seems to increase fracture visibility in some cases (Figure 2.3). Water cleans the face of dust and also can provide increased contrast between fractures and intact rock.

Another technique is to use a more viscous fluid that will concentrate in the fractures. If the fluid has a vivid color of florescence, this can be used to highlight the fractures. Experiments were conducted (Devgan and Kemeny, unpublished) using liquid detergent mixed with fluorescent dye. The face was then photographed under fluorescent light. Certain liquid detergents contain fluorescent materials, and also they are very viscous. The viscous detergent tends to concentrate in the fractures. In order to contrast with the intact rock, the face was rinsed with water, so that the dye and soap mixture

remained only in the fractures. This procedure was unsuccessful, since the rinsing also removed the detergent from the fractures. Another method tried was using infra-red film with a 35mm camera. Assuming that fractures would heat or cool at a different rate than the intact rock, the fractures should be enhanced by the infra-red film. The results of this method as well as other methods are still being investigated.

CHAPTER 3

VIDEO IMAGING PROCEDURES AND EXPERIMENTS

This section describes the specific procedures used in determining size distributions using a video camera and a computer with digital image processing software. This section also discusses experiments that were conducted to validate the video imaging technique.

3.1 Overall Procedure for Video Imaging

The method used to obtain the images of fragmented rock particles is shown in Figure 3.1. As shown in the figure, the images are taken in the field with the help of a video camera. To obtain better images it is advised to mount the video camera on a tripod. This will hold the camera steady and produce better quality images. Care should be taken to take images in such a fashion that the rock particles imaged are either totally in the sun or totally in the shade. If an in-between situation is chosen, it is difficult to delineate the rock particles satisfactorily. Care should also be taken to keep the video camera perpendicular to the rock face being imaged. If this is not done, the particles away from the camera appear smaller than their actual size and those closer to the camera appear larger then their actual size. If an angle between the camera axis and the slope cannot be avoided, then processing can be performed to correct for the angle.

After taking images in the field, the tape is viewed on the computer to pick out the images for processing. Images are taken at different scales to take into account the large variation in fragment sizes. The criteria for picking images for processing is as follows:

- A number of images are taken in order to take into account the heterogeniety of the rock fragments.

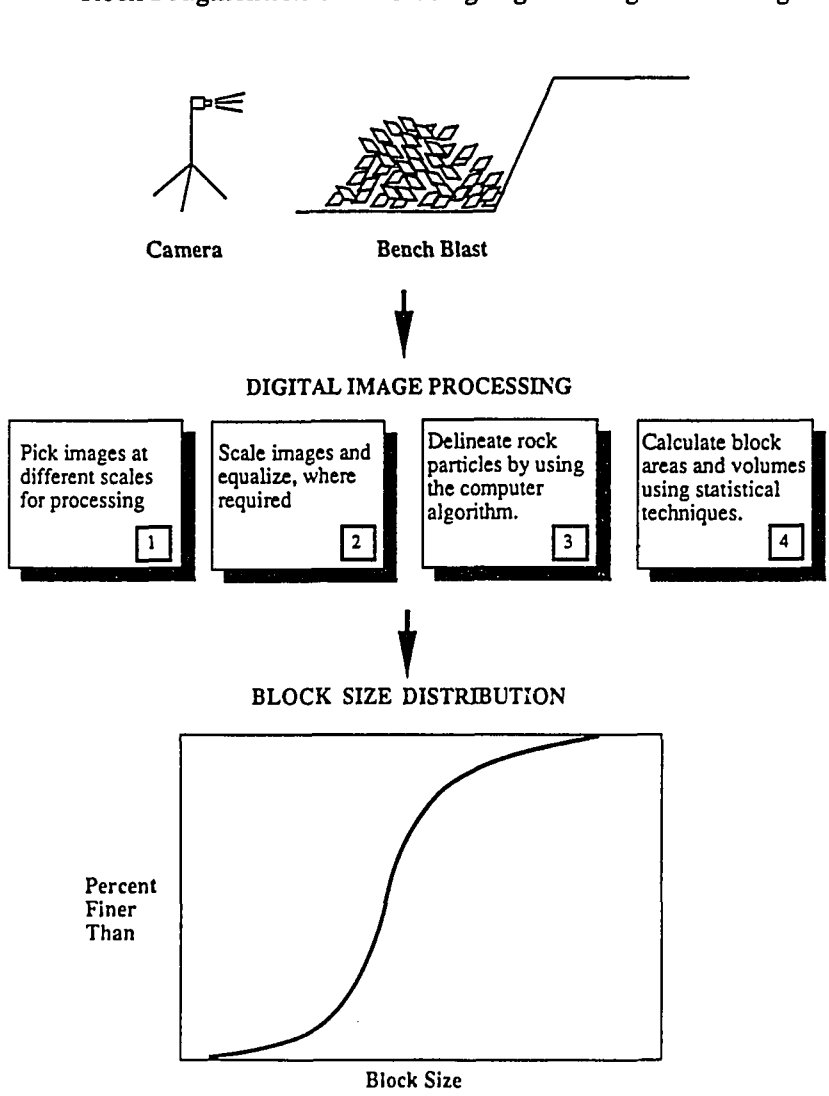

Figure 3.1 : Outline of the method used to obtain images of fragmented rock particles.

- Images are taken at different scales.

- Images are taken that are clear, steady and have uniform lighting.

The sampling error associated with taking a certain number of images can be quantified, as discussed in section 5.1.

The next step is to scale these images. For this purpose a scale is always present in the image, preferably lying horizontally near the bottom of the image. This helps us in calculating the absolute size distribution curve, and not the relative size distribution curve. A variety of filters can be used to pre-process the image prior to the analysis. The most common reason for pre-processing the image is to correct for lighting problems. For instance, an image taken under low light conditions will be weighted towards darker gray levels. A simple equalization filter can be used in such cases to spread the light levels to all ranges of gray levels(0 to 255).

The third step is to delineate the rock particles by using computer algorithms. As described in section 3.3, the delineation of touching and overlapping rock particles is solved by a procedure based on two algorithms. The first algorithm analyzes the shape of the shadow boundaries located in void spaces and partially along the edges of fragments. This algorithm searches for relatively large gradient paths from sharp points in the shadow regions, and "splits" the particles along such paths. The first algorithm delineates most of the touching and overlapping rock particles, but does not delineate touching particles for which no large gradient path occurs. The second algorithm is used to find such undelineated rock particles and delineate them using a heuristic search along with a rock shape criterion. Both of these algorithms are described in greater detail in section 3.3.

In the fourth and final step, the block areas and volumes of the individual rock particles are calculated in order to determine the size distribution curve, by using statistical techniques. This is done after all the particles in the image have been

delineated and the image has been converted into a binary image. This then gives us the classical "S" shaped curve for size distribution as described by Noren and Porter (1974). Test results show that the method gives a high degree of accuracy, even in very complex rock conditions and under difficult light conditions. The statistical techniques are described in detail in chapter 4.

3.2 Causes for Sampling Error

The use of image analysis techniques for fragmentation analysis requires careful consideration of the three stages in the process; sampling, image acquisition and image analysis. Sampling concerns the taking of images that represent the blasted material being analyzed. Image acquisition concerns the taking of images which are of sufficient quality for the intended analysis process. Image analysis refers to the measurement of the size distribution of fragments identified in the image and corrected by stereological principles.

The three parameters affecting the sampling errors are type, scale, and number of images. The type of image refers to the location and state of the material being sampled and is the most important factor in capturing a representative image. Little substantive work has been done on comparing different types of image locations, although many differing ideas have been presented largely on the basis of field observations. Again, operational constraints dictate what methods can be used. In underground operations, photographs taken at draw points are often the only type available. In surface operations, photographs can be taken on the muck pile surface, at the digging face or of material in the back of haul trucks. Specific blasting conditions can dictate which of these is the most representative method of sampling. Consideration should also be given to the fact that random or systematic sampling is a requirement in order to minimize bias, and that some methods may be preferable in this respect (Hunter et al., 1990).

At any given scale, image analysis can measure fragments within a size range determined by the minimum resolvable size and the maximum visible size. The size range is dependent on the image analysis technique; the range achievable by tracing and digitization being larger than that for automatic methods. The minimum size is also dependent on the total resolution of the system, which is a function of environmental conditions, photographic scale, quality of image input and the inherent resolution of the image analysis. For a large fragment, the surface texture may cause the automatic methods to detect false edges to produce a group of small fragments. This is often termed "disintegration" and its occurrence depends primarily on rock texture and lighting conditions. A trade-off has to be found between the need to take close-up images in which fines can be resolved and the sampling error introduced by analyzing a reduced area of blasted material. It should also be noted that to achieve an adequate sample size with close-up images requires the analysis of an increased number of images thus increasing the processing time (Hunter et al., 1990).

An obvious conclusion from sampling theory is that the greater the number of images analyzed, the nearer the result will be to the truth. Empirical estimates have been made in the past of the minimum sample size necessary to be analyzed in order to achieve a given accuracy. However, consideration of sampling theory for particulate materials shows that the maximum expected fragment size determines the proportion of the material required to be analyzed for a given accuracy. It should be noted that the smaller fragment size fractions require less material to be sampled for good accuracy. Conclusions from sampling theory should not necessarily change the sampling technique but should allow the errors introduced to be understood and quantified. Most published work in image analysis gives good accuracy in the small to medium fragment size fractions, but even so it is recommended that some images containing the larger size fractions be taken (Hunter et al., 1990).

Video recorders can simplify image capturing for automatic methods but a high-quality recorder is required. This is why we used a high resolution video camera for our study. Initially image capture was being done by taking photographs in the field and then scanning them onto the computer by using a scanner. This method is more time consuming as the photographs have to be developed first before they can be analyzed. This also prevents real time processing of images. If sufficient computing power is available for real time analysis, images may be captured from a high-quality camera directly by the analysis computer.

Monochrome images are preferable for automatic methods where the contrast between fragment and background is the basis of particle identification. For artificial illumination factors such as intensity, direction of lighting and diffused lighting should be considered. Generally angled lighting increases the contrast but also increases disintegration of the image during analysis (Hunter et al., 1990). For this study all the images were taken in the sunlight, and the lighting angle was close to perpendicular to the rock face.

In general, blasted material that requires analyzing lies at an angle to the horizontal so some consideration should be given to the relative angle of the camera axis. The ideal is to produce an image of constant scale which requires the camera axis to be perpendicular to the surface of the material. It is unlikely that any of the analysis methods are very sensitive to small deviations from the perpendicular. If this is not feasible, two scale markers can be used with the image being analyzed in two portions at different scales. Normally one scale marker is used, although if a batch of photographs are to be taken at a constant distance from the camera, for example, on a conveyor belt, then only the first image requires a marker (Hunter et al., 1990).

Manual image input involves manual digitizing of the particle outlines from a photographic print or automatic digitization of a tracing of the particle outlines.

Automatic image input allows the computer to identify the particle outlines often with some manual post-editing. The image processing techniques used to achieve this vary, however good contrast between particles and background is required to ensure accurate results. We are using automatic input of images with no manual editing in most circumstances. This is described in section 3.3.

In large open pit mines, blasting is a high cost area which often has very little feedback on performance. Methods of fragmentation analysis offer quantitative measurement of blast performance and thus open the door to effective optimization of the blasting process. The alternatives to image analysis for fragmentation measurement are either subjective or time consuming (Hunter et al., 1990). In an open cast mine, blasted material can be sampled either before digging (the muck pile surface), during digging (at the face), or while in haul trucks or on a conveyor (after crushing). A suitable site can be chosen depending on the needs and availability of the mine.

The most important characteristics of the video imaging technique can be summarized as follows. This summary indicates the degree of difficulty involved in successfully delineating all the fragmented rock particles.

(a) The rocks overlap and hide portions of one another.

(b) Occasionally a large rock looks like a group of small rocks, and groups of small rocks look like large single rocks.

(c) The surface of these rocks ranges from very smooth to very rough. The rocks can be described generally as having convex surfaces, but they may have many ridges, indentations, and other features on their surfaces.

(d) The rocks are 'randomly' oriented, but there are packing patterns.

(e) The rock particles cast shadows, making it difficult to delineate the fragments in the shadow region.

(f) The muck pile may be at an angle to the camera.

(g) There may be lighting problems; for instance, the top of the image may be light but the bottom may be dark; or the entire image may be dark, as in underground photos.
(h) Weathering causes small particles to be washed away, leaving a larger percentage of large particles.
(i) Gravity causes large particles to move to the bottom of the slopes, leaving fines near the top.
(j) The range of fragment sizes may be over many orders of magnitude.

3.3 Particle Delineation

This section describes the specific algorithms used to delineate the individual rock fragments in the digital images. As stated previously, this is an important first step in estimating the size distribution.

3.3.1 Algorithms for Fragment Delineation

A characteristic of fragmented rocks is the large percentage of the volume taken up by void space or porosity (10-40%). Under natural light, these void areas will appear as dark or shaded areas. These dark areas will partially but not completely outline the boundaries of the rock fragments. In particular, where the shadow regions meet with particle edges, the shadow regions will form sharp convex shapes with angles that point in the direction of the edge between the touching particles. This is shown in the sketch below.

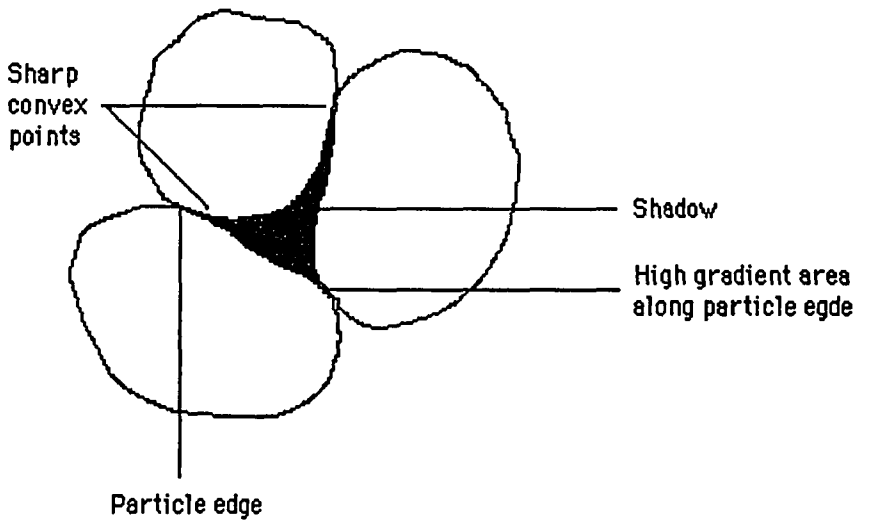

These sharp convex-shaped shadows can also be seen in Figures 2.1 and 2.2. In the region where the rock fragments touch, there usually will be relatively large gray-level differences due to the particle edges. In almost all cases, there is at least some gray level difference between touching rock fragments.

A procedure has been developed for automatically delineating individual rock particles. The procedure takes advantage of the shadow regions that occur in the void spaces and the large gray-level differences that occur along the edges of touching particles. The procedure is based on two algorithms. The first algorithm analyzes the shapes of shadow regions and searches for large gradient paths in the region ahead of sharp convexities in the shadow regions. As discussed in section 2.1 gradient value for a pixel is a measure of the contrast in gray level between the pixel and neighboring pixels. A high gradient value may indicate the presence of a boundary of a fragment. The gradient value alone is not a good edge detector, since noise will also cause a high gradient. The basis for Algorithm 1 is as follows:

(1) The gradient values along the touching areas of particles are assumed to be larger than some threshold value;

(2) The shadow boundary in the void space between particles tends to form convex regions that point in the direction of edges;

(3) The rock particles under consideration are larger than some noise threshold.

Algorithm 2 is be used to find clusters of undelineated touching particles whose gradient values along the touching areas are less than a prescribed gradient threshold value (i.e., where assumption 1 does not hold.) and delineate touching particles using a heuristic search(see Gonzalez and Wintz, 1987). The basis for Algorithm 2 is as follows:

(1) Cluster regions of touching particles are simply-connected(i.e. they do not contain holes).

(2) A cluster boundary at points where rock particles touch tends to form concave regions.

(3) The length between two touching particles is relatively short compared with each individual particle perimeter on the either side of the touching path.

As an example of the use of these two algorithms, Figure 2.2 shows the delineated rock fragments from the rock image in Figure 2.1. Figure 2.2 shows that the algorithms are able to delineate fragments with a high degree of accuracy, even for the complex conditions shown in Figure 2.1. Details of these algorithms are given in Wu and Kemeny (1992).

The algorithms described above have been implemented into the image processing package called *Image* developed by the National Institutes of Health (NIH). NIH *Image* is a public domain program that supports a number of standard image processing features.

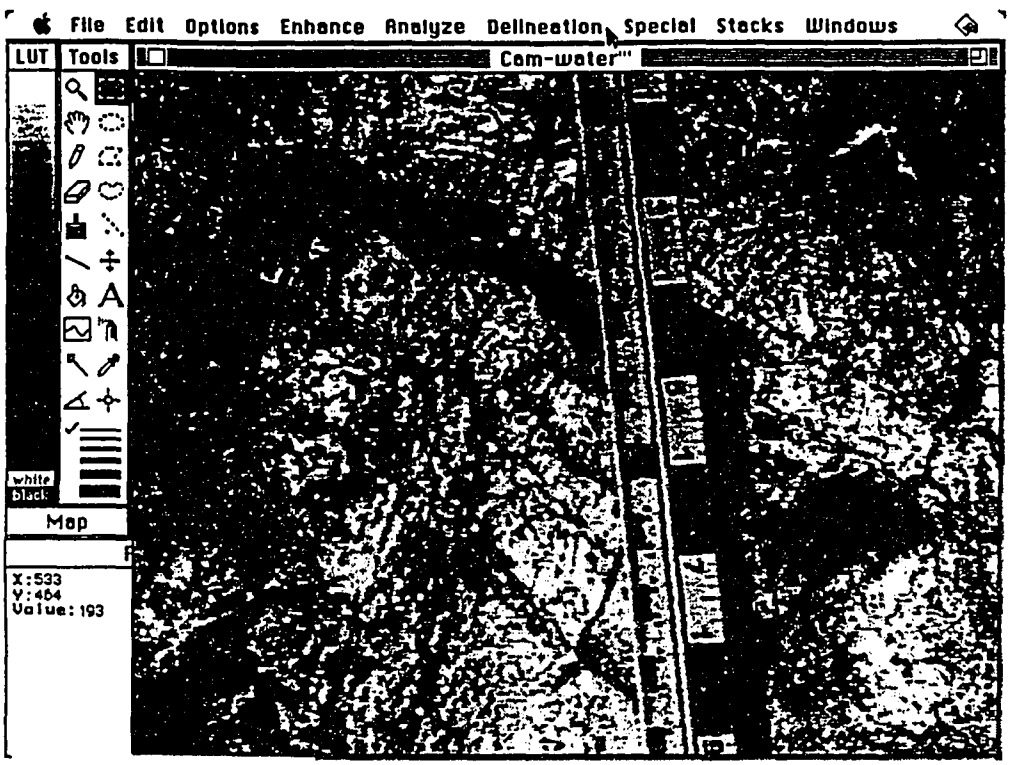

Figure 3.2 : Example of a screen in NIH *Image*.

Figure 3.2 shows a screen in NIH *Image* and also shows the delineation menu that has been added for performing automatic fragment delineation.

3.3.2 Fragment Shapes and Areas

After the fragments have been delineated, various shape and size information are calculated for each fragment. The NIH *Image* program has built-in routines to calculate the following information on each fragment: area, best-fitting ellipse (maximum diameter a, minimum diameter b, angle θ), perimeter, and position. This information is used in the next section to determine statistical parameters.

3.4 Validation Experiments

Laboratory experiments were carried out to determine the relationship between size-distributions as determined from two-dimensional video images, and the actual three-dimensional size distributions as determined by sieving. Blasted rock fragments of metamorphosed limestone were obtained for this study from the University of Arizona San Xavier mining laboratory. 107 kilograms of rocks were used in this study. These rock fragments were initially sieved in the laboratory using screens of the following five sizes: 0.5, 1.0, 1.5, 2.0, and 2.5 inches. The relative weight of the fragmented rocks in six categories (<.5, .5-1, 1-1.5, 1.5-2, 2-2.5, >2.5) were measured as shown in Table 1.

Data obtained from sieve analysis in the laboratory

	< 0.5 in	0.5 - 1.0	1.0 - 1.5	1.5 - 2.0	2.0 - 2.5	> 2.5
Relative Weight (%)	40.44	22.51	12.86	9.05	6.68	8.46

Two kinds of experiments were performed. In the first set of experiments, images were taken of the rock fragments in some of the individual size classes. This was done to correlate fragment size with information from the two-dimensional images. In the second set of experiments, images of the overall distribution were taken after the rocks were re-mixed.

3.4.1 Images of Individual Size Classes

One of the important factors was to find a way to quantify the "size" of a rock fragment based on the information obtained from the two-dimensional images. As described in the previous section, this information includes the fragment area, and the major and minor axes of the best fitting ellipse. In this thesis we correlate this information with the screen size for the rock fragment. The screen size for a rock fragment is defined as the length of the square grid that just allows the fragment to pass. The screen size depends on the minimum and intermediate dimensions of the rock fragment but not the maximum dimension. The average size in each class interval (taken to be midpoint of the interval) was compared with different measures from the two dimensional images. These included the square root of the area, the major axis, the minor axis, the average of major and minor axes, and different linear combinations of the major and minor axes.

In order to determine how fragment size is related to the various image parameters, experiments were carried out in the laboratory. Fragmented rock particles were sieved in three size categories of 1.0 - 1.5 inches, 1.5 - 2.0 inches and 2.0 - 2.5 inches respectively. These size classes contained enough particles to represent all the possible shapes of rock fragments found in a full-scale blast in the field. After images of each class had been processed, we had 633 particles of known sieve size. These included 240 particles in the sieve size 1.0 - 1.5 inches (Figure 3.3), 276 particles in the

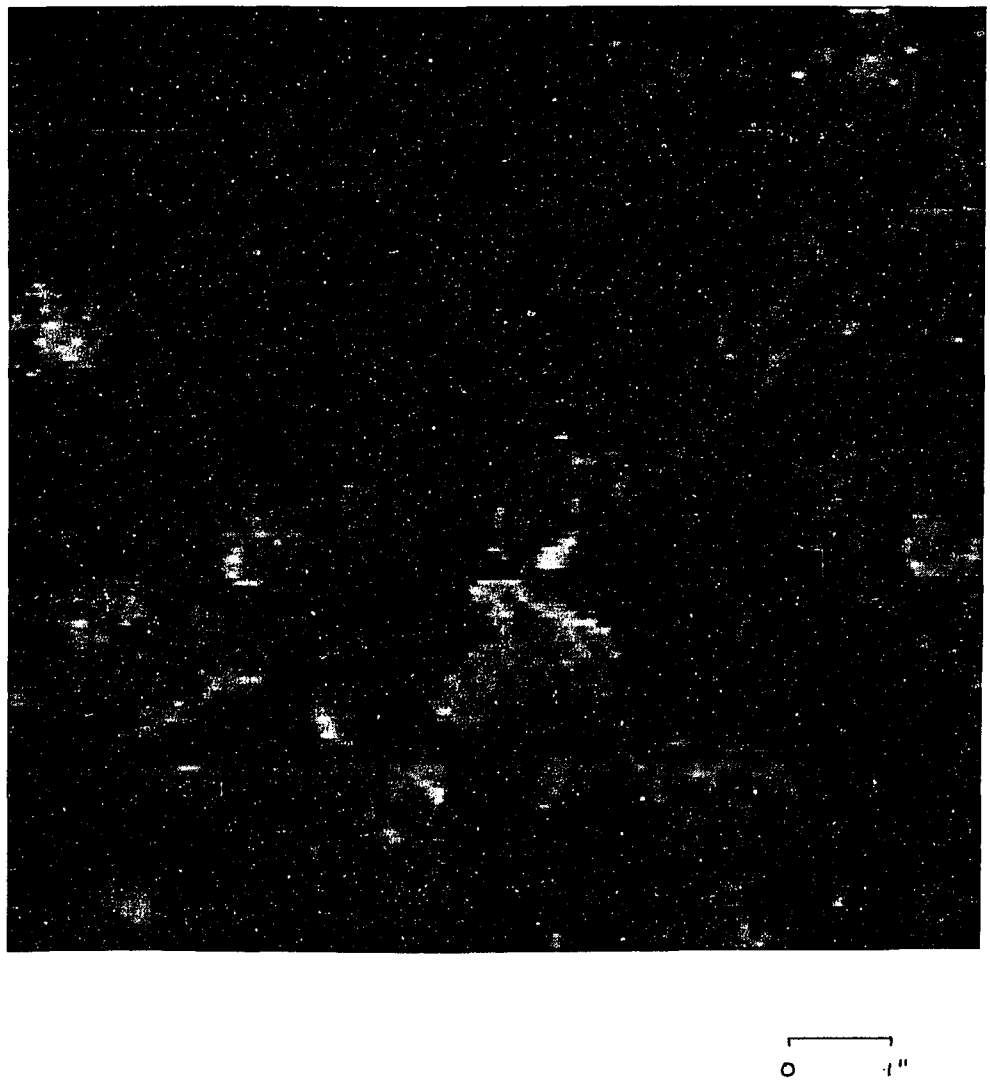

Figure 3.3 : Images of Individual Size Class. All particles in this image belong to the size class 1.0 - 1.5 inches.

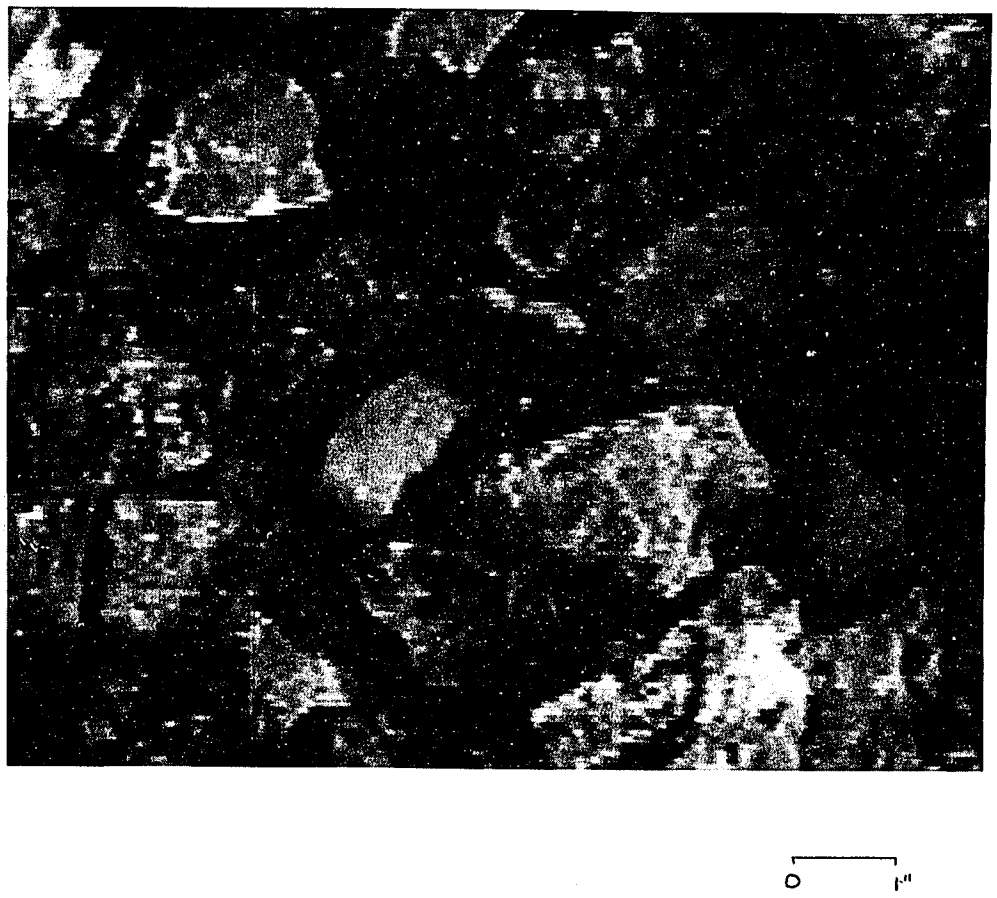

Figure 3.4 : Images of Individual Size Class. All particles in this image belong to the size class 1.5 - 2.0 inches.

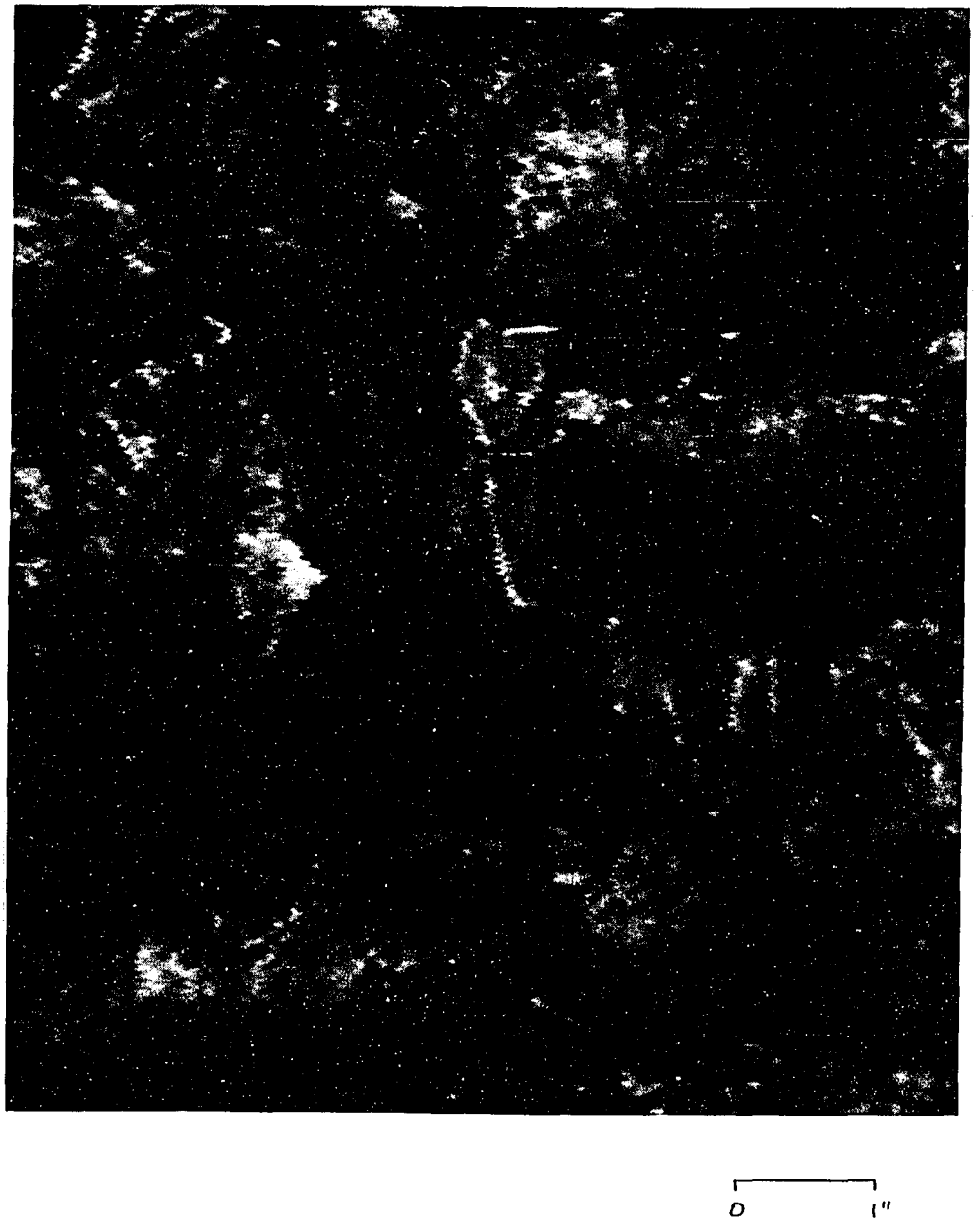

Figure 3.5 : Images of Individual Size Class. All particles in this image belong to the size class 2.0 - 2.5 inches.

sieve size 1.5 - 2.0 inches (Figure 3.4), and 117 particles in the sieve size 2.0 - 2.5 inches (Figure 3.5). Since the size of each class interval was known, the results from the processed images were compared to each of these sizes. This gave us three different class intervals to correlate and determine an empirical formula which would relate the average size of the particles in one particular category to the combination of major and minor axes of the ellipse that the computer program had fit through each of the delineated particles. From this analysis an empirical formula was determined that gives the fragment size as a linear combination the minimum and maximum axes of the best fitting ellipse through the fragment. The results of this analysis are described in chapter 4.

3.4.2 Images of the Mixed Rock Fragments

In this set of experiments the screened rock fragments were re-mixed, and images were taken from small muck piles that were made of the mixed rock fragments. The purpose of these experiments was to compare the size distribution determined from image processing of the video images with the actual size distribution determined from the screening. For this purpose the total 107 kg of rock was divided into two sets. For each set, muck piles were made and images were taken with the video camera. Examples of these images are shown in Figures 3.6, and 3.7. In order to take into account sampling variability, five images of each set were taken. After each image was taken, the rocks were mixed thoroughly and a new muck pile was made.

In addition to capturing a number of images to take into account sampling variability, images were taken at different scales. The size of rock fragments in the experiment varied from less than 0.1 inches to about 6 inches. Since the resolution of the video images is limited (640 x 480 pixels), a procedure has been developed for combining the size information taken at different scales. For the experiments performed

Figure 3.6: Images of the mixed rock fragment. This is one of the images from the first set.

Figure 3.7: Images of the mixed rock fragment. This is one of the images from the second set.

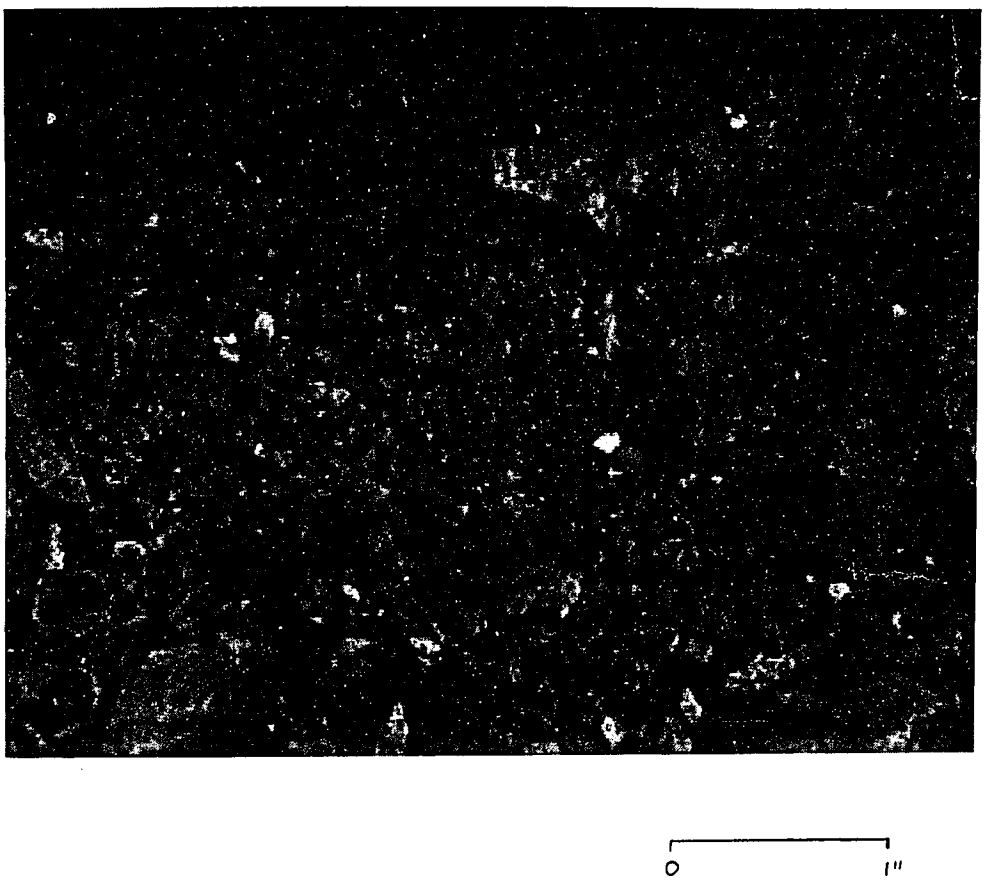

Figure 3.8 : One of the zoomed-in images of the fines in the muckpile.

in this section, images were taken at different scales by adjusting the zoom lens on the video camera. Figure 3.8 is an example of an image of fines that have been zoomed-in. Images in the largest scale contained the largest fragments on the surface of the muck pile, and fragments in the smallest scale image were such that the smallest fragments could be delineated using the algorithms described in section 3.3.

CHAPTER 4

STATISTICAL ANALYSIS

We obtain two dimensional information from the video images, but we need three dimensional information from these images to obtain the size distribution curves. In particular, the size distribution curve depends on the volume of each of the rock fragments. We therefore need some statistical techniques for correctly characterizing the three dimensional volumes of the fragments from two dimensional images. The second factor is that we take images at different scales, in order to take into account both the smallest and largest fragments. Statistical techniques must again be used to correctly combine information from different images to obtain the true size distribution of the fragments.

4.1 Screen Size Determination for each Fragment

Not all the particles that are imaged with the video camera represent the true shape and size of the actual particle. The actual size of the particle may be bigger or smaller than the apparent size as seen in the image. The shape and size of the particle has to be taken into account in order to correctly determine the size distribution. As stated previously the sieve size of a particle depends on its minimum and intermediate dimensions, but not on the longest dimension. Depending on how the fragment is oriented in the muck pile, we may be seeing any combination of its three principal dimensions. For example, consider a rectangular parallelepiped with dimensions 1 x 2 x 8 inches.

The figure below shows the three ways that the block might appear in two dimensions.

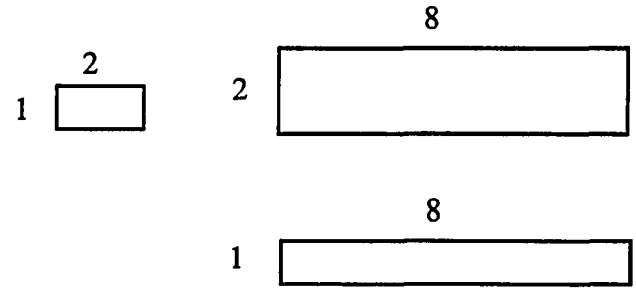

For this case, more likely than not the particle will be assigned a sieve size bigger than its actual sieve size(2 inches in this case). Another important factor is the effect of fragments partially covering other fragments. This will cause the sieve size for a fragment to be underestimated. These are the problems that need to be considered while conducting statistical analysis.

After processing the images with the help of the particle delineation algorithm, we obtain the area of each particle, and the major and minor axes of the best-fitting ellipse. This information is used to determine the volume of each particle. Also, we want to obtain the probability for each particle belonging to a particular size category or class. We shall then use this information to calculate the size distribution.

The first task was to develop an algorithm which would assign to each imaged particle a probability that the particle belongs to each of a set of specified size categories. Images were taken of muck piles made up of individual class sizes: 1.0-1.5, 1.5-2.0, 2.0-2.5 inches. First, using images of 633 particles of known sieve size (240 particles from sieve size 1.0 in - 1.5 in, 276 from size 1.5 in - 2.0 in, and 117 from size 2.0 in - 2.5 in.), the minor axis, major axis, and area of each particle were

measured. Assuming that the midpoint of a sieve size is a reasonable measure of the average dimension of a particle in that size category, a function of these three imaged dimensions whose average matched the average true dimension was sought. Trial and error produced the function:

$$d = 0.45 * \text{major axis} + 0.73 * \text{minor axis}. \quad (1)$$

The average of d for particles in each sieve size differed from the midpoint of the sieve size by at most 0.017 in. (0.76 %). In all further analysis, d was used as the linear dimension of imaged particles.

Although three specific sieve sizes were used to develop the algorithm, we wanted an algorithm that could be applied to any set of equally-spaced size categories. To make the algorithm independent of actual particle size, each observed particle size must be scaled to a relative particle size. Since we had three sieve sizes, we used the midpoint of the 1.5 - 2.0 in. size (1.75 in) to scale all the observed particle sizes.

4.2 Correction of Screen Size for Overlap and Fragment Shape

Next, frequency distributions of relative particle size ($x = d/1.75$) were tabulated for the particles belonging to the three sieve sizes. Bins of size 0.1 inch were used for this frequency distribution. Larger bins would have resulted in too few points for the curve-fitting described below; and smaller bins would have had too few particles per bin to give stable estimates of the frequencies. Since there were different numbers of particles in each size category, the cell counts were normalized by dividing by the total number of particles imaged in the respective sieve size. This gave the proportion of particles of a given known sieve size that fell in the relative size range $(x, x + 0.1)$. We were interested in a different proportion, however. We wanted to know, for a particular relative particle size, the proportion of the particles that belong to each sieve size. To

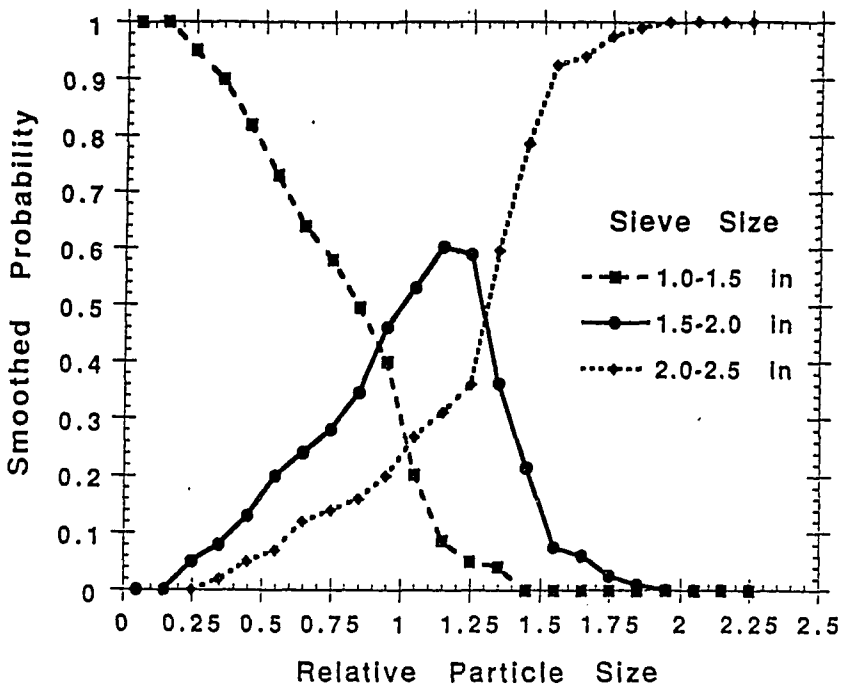

Figure 4.1 : A plot of the observed probabilities versus the midpoints of the relative particle size.

compute these proportions, simply divide the normalized cell counts for each relative particle size by the sum across sieve sizes of the normalized cell counts. For example, for the relative particle size $0.8 < x < 0.9$, there were 25 out of 240 particles in the smallest sieve size, 39 of 276 in the middle sieve size, and 4 of 117 in the largest sieve size. Thus,

$$f_1 = \frac{25/240}{25/240 + 39/276 + 4/117} = 0.3725$$

$$f_2 = \frac{39/276}{25/240 + 39/276 + 4/117} = 0.5053 \qquad (2)$$

$$f_3 = \frac{4/117}{25/240 + 39/276 + 4/117} = 0.1222$$

Note that $f_1 + f_2 + f_3 = 1$. (A particle must belong to one of the three sieve sizes.)

A plot of these observed probabilities versus the midpoints of the relative particle size groups produces three curves, one for each sieve size (Figure 4.1). To predict the probability that any imaged particle belongs to a given sieve size, all we need are equations that fit these observed curves. In fact, since $f_1 + f_2 + f_3 = 1$, all we need to do is fit two curves and calculate the third as 1 minus the sum of the first two. Since the curve for f_2 is more complicated to fit than those for f_1 and f_3, we chose to calculate the f_2 equation form the f_1 and f_3 equations. The best fitting curves (Figure 4.2) were:

$$f_1 = -0.0525 + \left(0.9898 + 2.1581x^{3.9574}\right)^{-1}$$

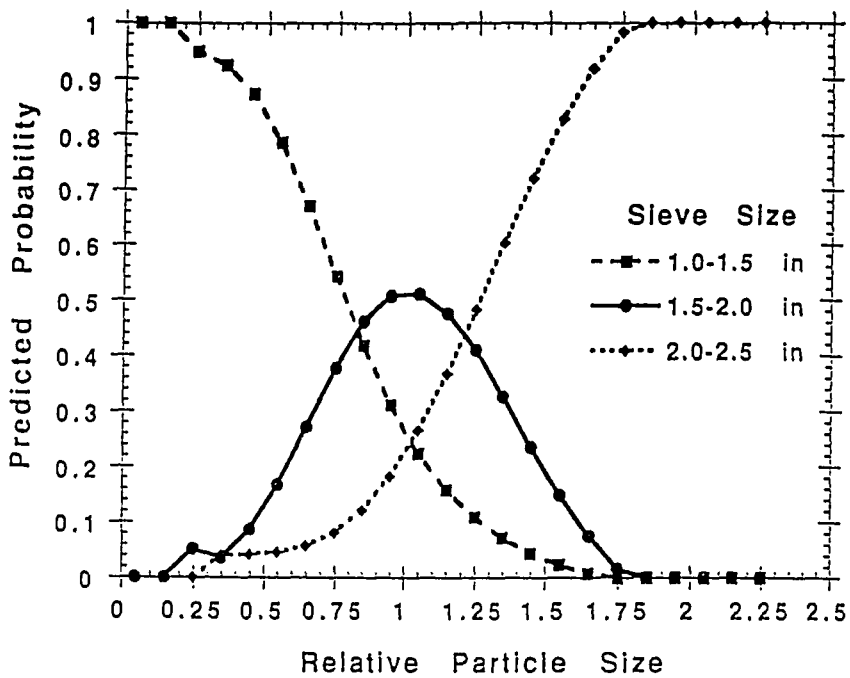

Figure 4.2 : The best fitting curves for the plots in Figure 4.1.

If $x \leq 0.2$ or $f_1 > 1$, set $f_1 = 1$; and if $f_1 < 0$, set $f_1 = 0$.

$$f_3 = 0.0401 + 20.8973x^{9.3084}e^{-4.7464x} \qquad (3)$$

If $x \leq 0.2$ or $f_3 < 0$, set $f_3 = 0$; and if $f_3 > 1$, set $f_3 = 1$.

$$f_2 = 1 - (f_1 + f_3)$$

The curve fitting for equation (3) was performed with the help of a computer program called KaleidaGraph. It uses the method of least squares to fit these curves. The program was given equations of the following form to fit:

$$f_1 = C_1 + 1/(C_2 + C_3\, x^n)$$

where, C_1,C_2,C_3, and n were constants to be determined, and

$$f_3 = C_1 + C_2\, x^n\, e^{k.x}$$

where C_1,C_2,n, and k were constants to be determined.

These results can be expanded to an arbitrary number of equally spaced size categories using the following algorithm:

1. For each imaged particle calculate the area, minor axis, and major axis of its image. Then calculate

   d = 0.73 * minor axis + 0.45 * major axis

2. Select a set of k equally-spaced size categories and calculate the midpoints of categories (bins) 2 through k - 1 (m_2, m_3, . . . , m_{k-1}).

3. For each particle i calculate the raw probabilities (p_{i1}, p_{i2}, . . ., p_{ik}) that the particle belongs to each size category as follows:

a. Bin 1:

$x_i = d_i/m_2$

$p_{i1} = f_1$.

b. Bins 2 through k-1:

$x_i = d_i/m_j \quad j = 2, \ldots, k-1$

$p_{ij} = 1 - f_1 - f_3$

If $p_{ij} < 0$, set $p_{ij} = 0$; and if $p_{ij} > 1$, set $p_{ij} = 1$.

c. Bin k:

$x_i = d_i/m_k$

$p_{ik} = f_3$.

4. Normalize the probabilities so that for each particle they sum to 1:

$$P_{ij} = p_{ij} \Big/ \sum_{j=1}^{k} p_{ij} \qquad (4)$$

P_{ij} is the probability that the particle i belongs to size category j.

4.3 Calculation of the Overall Size Distribution

From these probabilities, various histograms can be derived. For example, to generate a % by volume histogram, multiply P_{ij} by an estimate of the particle's volume, sum over all particles, and normalize:

$$V_j = \frac{\sum_{i=1}^{N} v_i P_{ij}}{\sum_{j=1}^{k} \sum_{i=1}^{N} v_i P_{ij}} \qquad (5)$$

The volume of each fragment was estimated by taking the area of the fragment and multiplying the area by some linear dimension. The following four methods were considered in estimating the volume of each fragment:

1. Volume = Area * Minor Axis
2. Volume = Area * Major Axis
3. Volume = Area * (Major + Minor)/2
4. Volume = Area * (0.45*Major + 0.73*Minor)

The optimal method was determined by comparing the results with actual sieve analysis as described in chapter 5.

4.4 Combining Images Taken at Different Scales

Now suppose we have histograms derived from several images, and we want to combine them into one histogram. This problem would arise, for example, if we had images of a set of particles taken at more than one scale. We combine the images by weighting them by their areas when we add the histograms. Suppose we have n images with areas $A_1, A_2, \ldots, A_n$. Let V_{ij} be the % by volume in size category j for image i. Then the composite % by volume for size category j, V_j, is:

$$V_j = \frac{\sum_{i=1}^{n} V_{ij}/A_i}{\sum_{i=1}^{n} 1/A_i} \qquad (6)$$

CHAPTER 5

RESULTS AND CASE STUDIES

The size distribution obtained from the video images by using the procedure described in the previous chapters was compared with experimental sieve results given in Table 1 of chapter 3. As mentioned earlier 16 images of limestone fragments were taken. Out of these 16 images, 6 were zoomed images of the fines. Figure 5.1 is a histogram of relative weights in each of six class sizes, from the laboratory results as well as the procedures described in previous chapters. As described in chapter 4, four methods were used in estimating the volume of each rock fragment. Figure 5.1 shows that all four methods give a reasonable estimate to the sieve results. The one in which the volume is estimated as the fragment area multiplied by the size parameter given in equation (1) fits the data the best. Using this method, the cumulative size distribution is compared with the sieve result in Figure 5.2. The comparison is good, and shows the applicability of our method.

The size distribution obtained from the above mentioned procedure considers the overlap of fragmented rock particles while in a muck pile. It also considers that all the images have not been taken at the same scale. Some of the images of the fines were zoomed-in to better represent the size distribution. Figure 5.3 shows the cumulative size distribution curve if the fines were not included. The fines are significantly underestimated in this case.

The images were taken from two sets of muck piles which represented rock fragments obtained from a single blast. Enough images of each muck pile were taken to avoid any sampling errors. Since the whole muck pile was imaged each time, bias in the sampling was avoided, as the position where the image is taken could effect the end

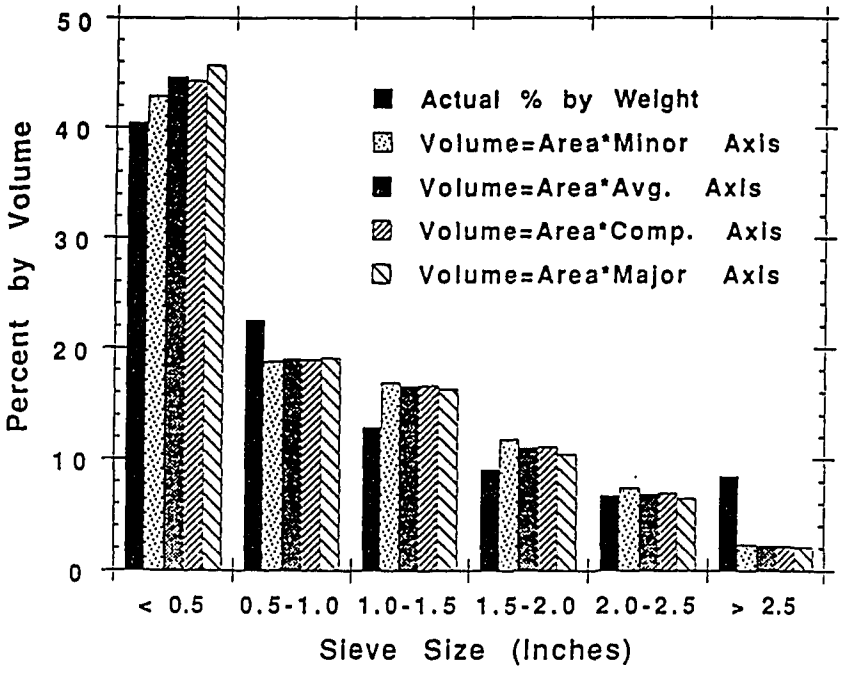

Figure 5.1 : Histogram of the relatives weights in each of six class sizes, from laboratory results as well as procedures described in this thesis.

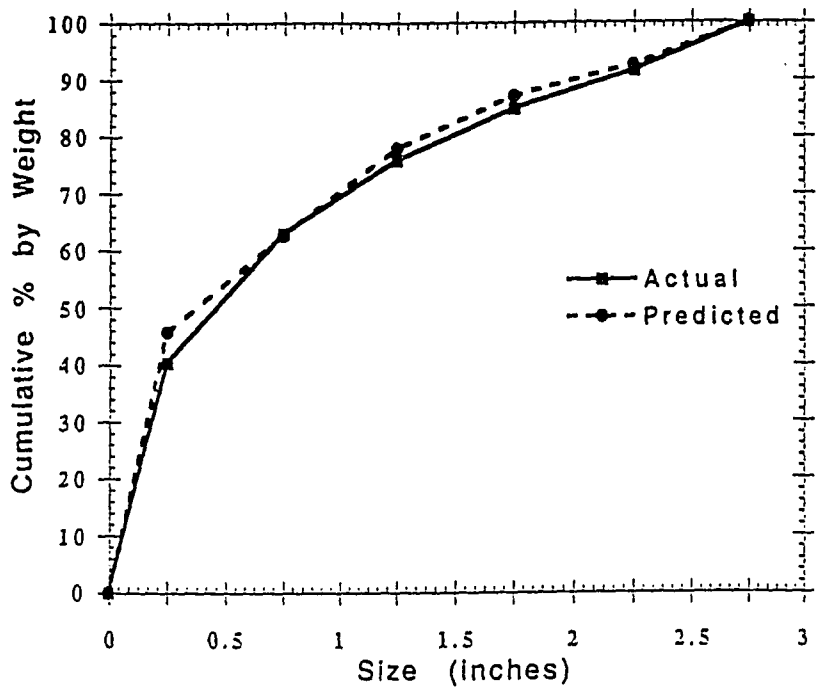

Figure 5.2 : Comparison of the cumulative size distribution with sieve results.

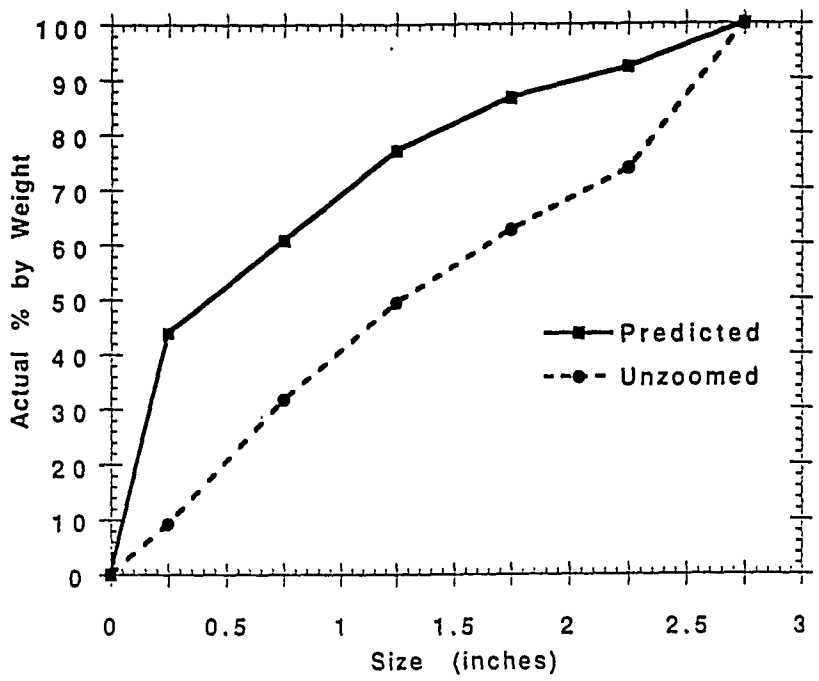

Figure 5.3 : Comparison of the cumulative size distribution with and without the inclusion of zoomed-in images.

results. The rocks were thoroughly mixed and poured into a muck pile before taking each image. An analysis of sampling is given in the next section. Also the video camera was always kept perpendicular to the face being imaged. Thus, errors due to a slope angle were avoided. Results obtained from this study show that digital image processing can be successfully used to obtain size distribution of rock fragments obtained after blasting.

5.1 Sampling Error Analysis

In this section, attempts to better understand the sampling error are described. Figure 5.4 shows a plot of the coefficient of variation for each of the six bins. The results are obtained by considering separately the unzoomed images and the zoomed images. The coefficient of variation is calculated as follows :

$$CV = \frac{S.D}{Mean}$$

where S.D stands for standard deviation. The higher the coefficient of variation, the more images that must be taken to get a representative average. From Figure 5.4 a number of conclusions can be drawn. First of all, the coefficient is large for the first bin size for the unzoomed images. This is because at an unzoomed scale, very few of the fines were imaged, leading to a large variation from image to image for this bin size. For the remaining bin sizes, the coefficient of variation tends to increase with the increasing bin size because fewer numbers of particles are present in the larger bin sizes. This can be seen from Table 1 on page 25. Apart from the first bin, the coefficient of variability for the rest of bins is around 0.2 for the unzoomed images. 10 unzoomed images were taken, which should be sufficient for this value of coefficient of variation.

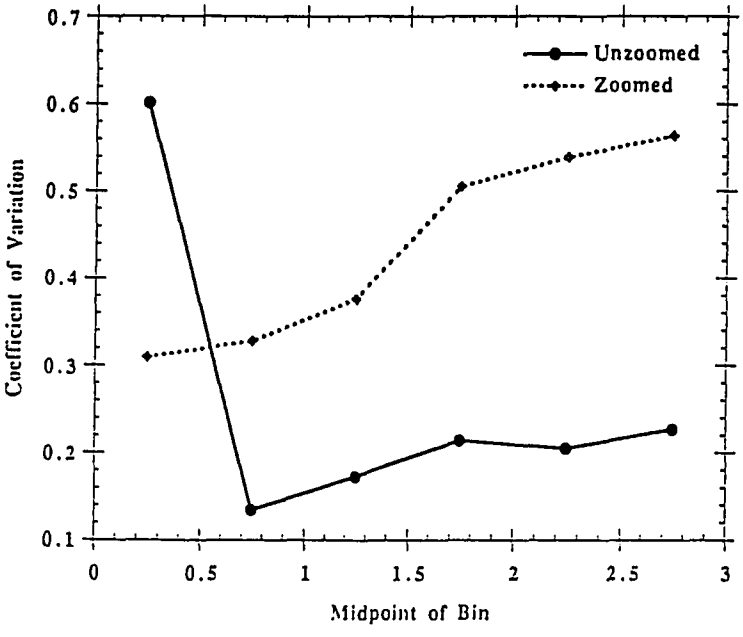

Figure 5.4 : Coefficient of Variation for Zoomed and Unzoomed images.

For the zoomed images, the coefficient of variation is around 0.35 for the smaller bin sizes and varies from 0.5 to 0.6 for the larger bin sizes. Again, high values for the larger bin sizes is a reflection of the inadequacy of the zoomed images to give information about the larger fragment sizes. The value of 0.35 for the smaller bin sizes is larger than the value of 0.2 for the unzoomed images. This is because the zoomed images sample a smaller section of the muck pile and are affected by the heterogeneity on a given pile. This indicated that, in general, more images should be taken at the zoomed scale. In fact, only 6 zoomed images were taken, which is probably not sufficient in this case. A more detailed study will be done in the near future to study the sampling errors generated due to this.

5.2 Case Studies

In this section two case studies are described that have been conducted in which our video imaging procedure has been used to determine the fragmentation. The first case study was conducted at the San Xavier Mining Laboratory and the second case study was conducted at the Cyprus Miami mine. These two case studies are described below.

5.2.1 Case Study at San Xavier Mining Laboratory

A high energy gas fracturing experiment was conducted at an abandoned shaft at the University of Arizona San Xavier Mining Laboratory on December 13, 1990. The purpose of the test was to produce a connection between the mine shaft and a vertical borehole drilled 15 feet from the shaft. A 450 lb., 36 foot fracturing experiment was fired between the depths of 108 and 142 feet. The result of the fracturing experiment was a complete connection between the borehole and the shaft at certain depths. The fragmented rock in this region moved into the shaft, and by removing this fragmented rock from the shaft, it was possible to analyze the extent of fragmentation.

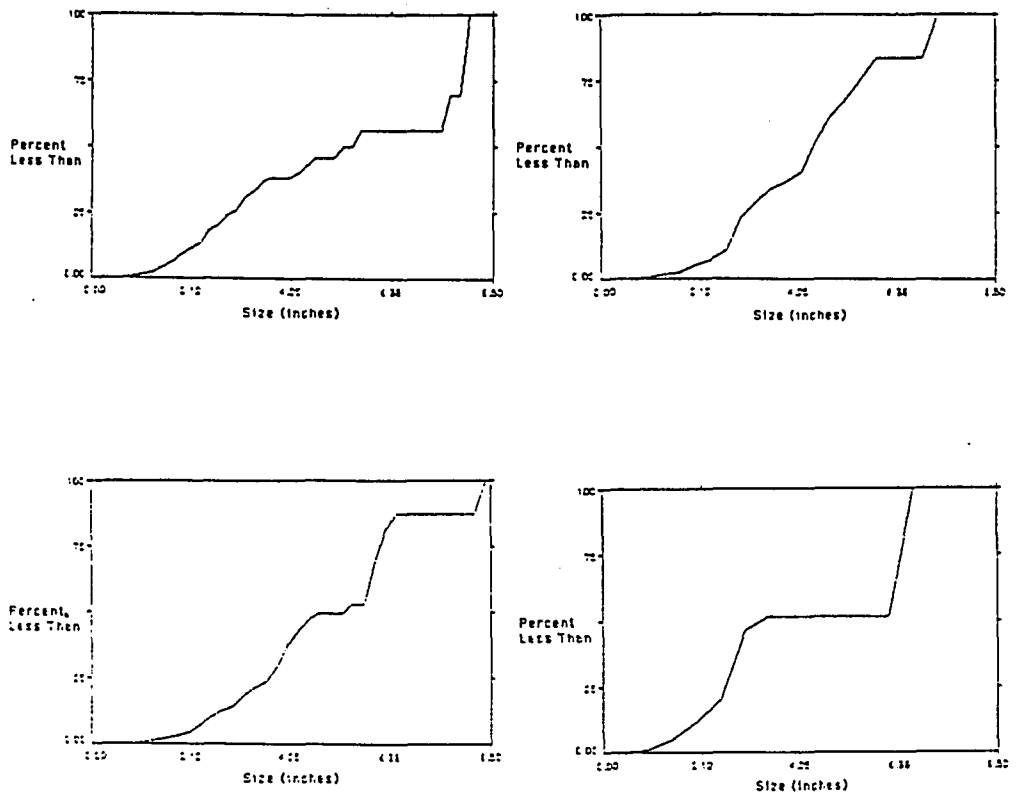

Figure 5.5 : Size distribution calculated for 4 of the images in the Case Study using the procedure outlined in this thesis.

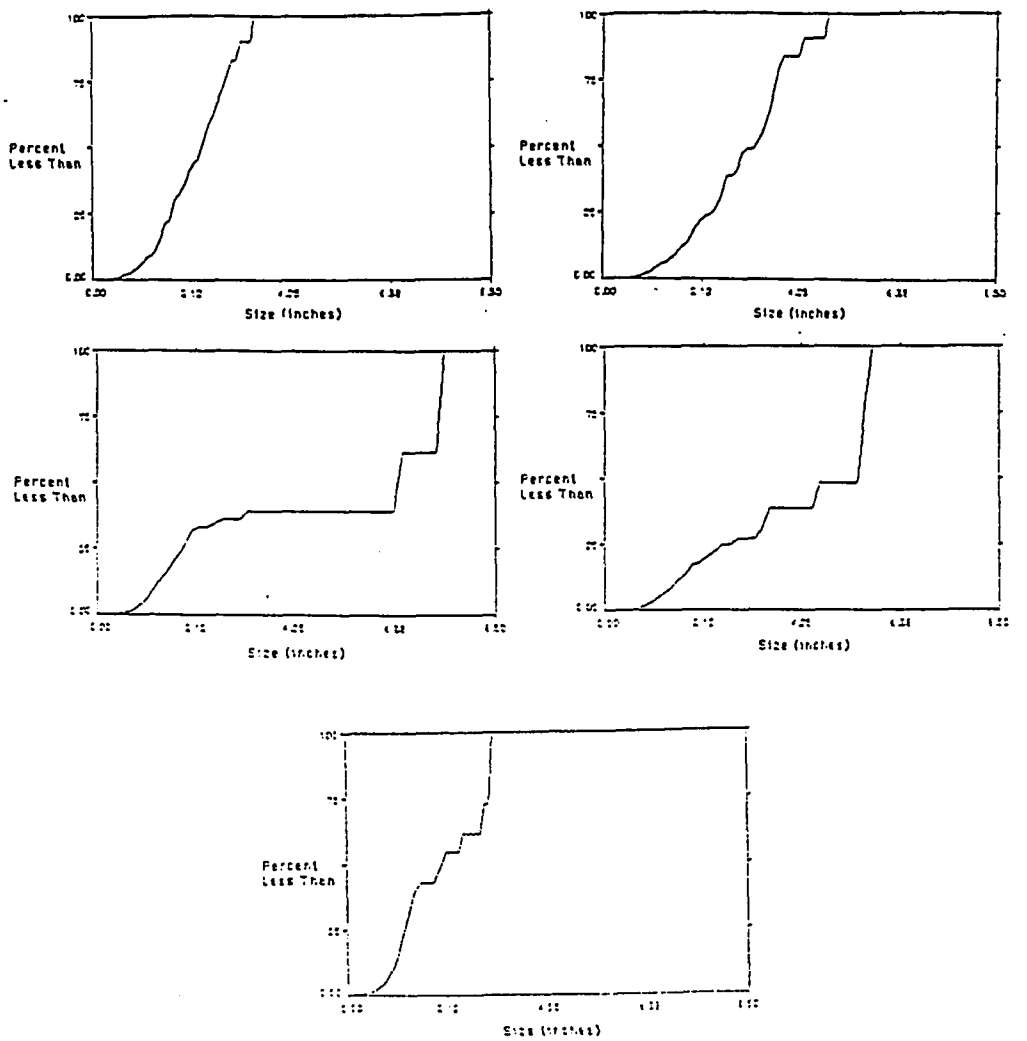

Figure 5.6 : Size distribution calculated for the other 5 of the images in the Case Study using the procedure outlined in this thesis.

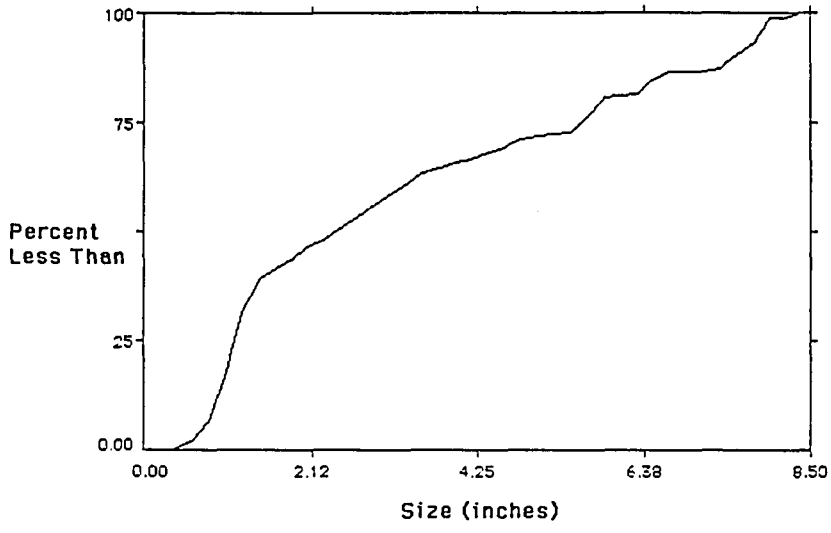

Figure 5.7 : Combined size distribution curve for all the 9 images in the Case Study.

Several field tests were conducted to give information on pre-existing fractures that existed prior to blasting. First of all, the borehole that was drilled at the site was examined using a borehole video camera. Secondly, a video camera was used in the shaft to give information on fracturing prior to the blast. The results from the downhole video camera were successful, and it gave limited but useful information on in-situ fracturing prior to blasting. Major fractures were seen over the whole range of depths where the blast was to be initiated, with fracture zones at depths of 123 and 129 feet. On average, at least 2 major fractures per foot were seen in the depth range of 106 to 144 feet. Many smaller fractures were also seen, but these were difficult to analyze from the video camera.

The rock fragmentation following the fracturing experiment was analyzed by examining the fragmented rock that was brought up from the bottom of the shaft. Rock fragmentation was analyzed from 9 photos taken from the recovered fragmented rock. Using the procedure outlined in this thesis the size distribution calculated from each of the nine images are shown in Figures 5.5 and 5.6. A combined size distribution curve of all 9 images is shown in Figure 5.7. The results indicate that good fragmentation was achieved in the fracturing experiment.

The photos scanned for the fragmentation analysis primarily focused on locations on the pile that had particles 8.5 inches in size or less. There were larger fragments that were retrieved, but good photos from these areas were not available. Also, it is difficult to compare the size distribution of the fragmented rocks after blasting with in-situ fracturing prior to blasting. One of the reasons is that information on small-scale fracturing in-situ was not available from either the borehole video camera or down-shaft camera.

Figure 5.8 : An example of one of the test samples for the Miami mine case study.

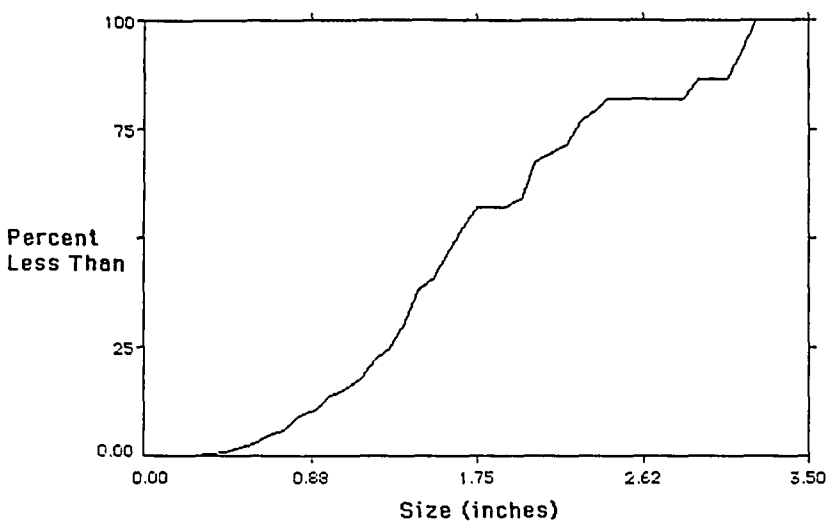

Figure 5.9 : Size distribution curve for the image shown in Figure 5.8.

5.2.2 Case Study at Cyprus Miami Mine

The second case study was carried out at the Cyprus Miami mine near Globe. The Miami mine primarily mines copper oxides which are processed by heap leaching followed by solvent extraction and electrowinning(SX/EX). Most of the heap leaching is performed on run-of-mine ore. The fragmentation due to blasting at Miami is therefore very important in determining the copper recovery that can be achieved by heap leaching. A study is presently being conducted in which water infiltration tests are performed on the top of an unleached pile. A number of infiltration tests were performed at random locations on the leach pile. After infiltration tests were performed samples of the rock at each test site were collected, and the size distribution of each sample was determined by spreading out the samples, taking video images, and using the analysis techniques described in this thesis. Figure 5.8 shows an example of one of the test samples, and Figure 5.9 shows the size distribution of this sample as determined by the procedure in this thesis. A comparison of the infiltration tests with the results of fragmentation analysis will be performed in the future.

CHAPTER 6

CONCLUSIONS AND RECOMMENDATIONS

6.1 Conclusions

The primary conclusion of this study is the development of a procedure for calculating the size distribution of rock fragments using video images. The procedure utilizes a high-resolution video camera for image capturing in the field and a set of computer algorithms for processing the video images. The computer program first delineates the individual rock fragments in the images. This is followed by a statistical procedure that takes into account fragment overlap and the two-dimensional nature of the images. More than one image at a time can be processed by the computer algorithms to produce a single size distribution curve. This procedure takes into account simple variability as well as combining images at different scales. By comparing the computer procedures with laboratory experiments, the accuracy of the method has been demonstrated for the case described in this thesis.

This is a simple and fast method of calculating size distribution of blasted rock fragments in the field. It is far less time consuming and expensive than the traditional sieving method.

6.2 Future Work and Recommendations

Based on the work discussed in this study, it is felt that the following aspects of analysis of rock fragments using digital image processing need to be investigated further:

1) The probability distributions(equations 3) were determined with a relatively small database of rock fragments. In the future these distributions should be recalculated with a larger data base.

2) In the near future, a field-scale calibration is being planned in a nearby open-pit mine. This will not only provide a larger database for statistical analysis, but will also serve the purpose of conducting the analysis on a different rock type.

3) Two important effects that have not been considered are the effects of gravity and weathering on the distribution of particles of different sizes on a rock slope. It is well known that gravity results in the larger particles moving towards the bottom of the slope, leaving a large percentage of fines in the upper portions of the slope. Also, weathering has the effect of washing away the fine material and leaving the larger size fragments on the slope. Field studies should be conducted to be able to take these effects into account in photographic analysis of the size distribution.

4) To have a better understanding of rock fragmentation and the factors that influence it, we also need to know the size distribution of the rock blocks before blasting. For this purpose, the pre-existing fractures and joint planes on the face of a bench need to be studied. Intersecting fractures and joints will form blocks, and from these the size distribution of the rock fragments before blasting can be calculated. Further research and experiments are required to fully automate the above procedure for calculating size distribution of blocks before blasting.

APPENDIX A

DATA FOR ONE OF THE IMAGES OF INDIVIDUAL CLASS SIZES

Image of Individual Class Size. All the particles in this image belong to the class size 1.0 - 1.5 inches. Area is the area of the particles in square inches. Major and Minor are the major and minor axes of the best fit ellipse in inches.

Area	Major	Minor
1.29288	1.59184	1.03412
0.42681	1.01580	0.53498
0.98135	1.33607	0.93520
0.44550	0.99886	0.56787
1.33494	1.63199	1.04149
0.78975	1.14851	0.87552
0.59815	1.09569	0.69508
3.15900	2.59577	1.54950
0.55765	1.23802	0.57352
1.08260	1.30997	1.05224
0.38008	0.90311	0.53585
1.11531	1.37976	1.02920
0.86919	1.37500	0.80487
0.13396	0.73367	0.23248
0.59971	1.07809	0.70827
0.48756	1.10765	0.56045
0.60127	1.00504	0.76172
2.38483	2.36438	1.28425
1.74617	1.67137	1.33022
0.32088	1.36164	0.30005
0.75081	1.08180	0.88367
0.44083	0.91671	0.61227
1.39569	1.83987	0.96585
1.97983	1.67949	1.50093
1.93777	2.11353	1.16736
1.79602	1.99433	1.14663
0.36294	0.81251	0.56875
0.75548	1.20387	0.79901
0.82558	1.66508	0.63130
0.91281	1.28897	0.90167
0.49535	1.33911	0.47098
2.40196	2.26211	1.35195
1.45333	1.73560	1.06616
0.70875	1.18700	0.76024
1.79913	2.08362	1.09940

0.71031	1.43430	0.63055
1.47358	1.93033	0.97197
0.62775	1.41982	0.56294
1.25550	1.50518	1.06203
1.09350	2.07606	0.67064
0.38319	0.98529	0.49518
1.15113	1.60138	0.91526
1.47358	2.40148	0.78127
0.46263	1.10560	0.53278
0.70875	0.98414	0.91695
1.25706	1.49616	1.06976
0.25079	0.85651	0.37281
1.81471	2.30934	1.00053
0.72277	1.20520	0.76357
0.77885	1.24191	0.79849
0.68383	1.02820	0.84680
0.95642	1.11185	1.09525
1.00315	1.50681	0.84765
0.70252	1.54336	0.57956
1.14646	1.76408	0.82747
0.15733	0.85525	0.23422
0.73056	1.26188	0.73713
1.45488	2.08093	0.89019
1.35363	1.58680	1.08615
0.75704	1.05938	0.90987
1.04833	1.37914	0.96783
1.39413	1.47616	1.20249
0.41590	0.89640	0.59074
0.34737	0.84710	0.52211
1.89260	1.81160	1.33016
0.96733	1.62806	0.75650
0.30375	0.74536	0.51887
0.37852	0.85212	0.56559
0.61217	0.96171	0.81048
1.35052	1.56363	1.09971
1.88325	1.98706	1.20672
1.33806	2.03065	0.83898
0.23054	0.68038	0.43142
1.08260	1.34180	1.02728
0.93773	1.36402	0.87532
1.60287	2.13208	0.95720
1.11687	2.13288	0.66672
0.32244	0.85863	0.47814
0.69785	1.36389	0.65147
1.02340	1.38588	0.94022
1.79290	1.73528	1.31552
0.59504	0.99043	0.76495
0.95487	1.56919	0.77478
1.40815	1.70308	1.05275
1.19787	1.63352	0.93367
0.60750	1.36154	0.56810

0.51404	0.90931	0.71977
0.63865	1.27866	0.63595
1.09662	1.50503	0.92772
1.75396	2.01926	1.10596
1.11687	1.51994	0.93559
0.89412	1.41422	0.80498
0.33335	0.78387	0.54145
1.46112	1.91140	0.97329
1.15581	1.30786	1.12521
0.48444	1.23950	0.49763
0.31154	1.00496	0.39470
0.99848	1.46954	0.86510
1.43152	1.95597	0.93185
1.71658	2.22651	0.98163
0.11527	0.60618	0.24211
0.53429	1.36340	0.49896
1.08260	1.36836	1.00734
2.05304	1.67109	1.56425
0.88321	1.21029	0.92915
0.36138	0.95232	0.48317
1.02652	1.50640	0.86763
0.30998	0.80359	0.49115
0.23521	0.79846	0.37507
0.77573	1.06438	0.92795
0.84427	1.20636	0.89107
1.22279	1.56852	0.99260
0.83025	1.74365	0.60626
1.48292	1.42316	1.32670
0.73367	1.03423	0.90322
1.67763	1.90683	1.12020
0.42369	0.92512	0.58312
0.64177	1.14948	0.71086
0.64800	1.25544	0.65719
0.50002	1.06728	0.59651

APPENDIX B

DATA FOR ONE OF THE IMAGES OF MIXED CLASS SIZES

Image of Mixed Class Size. All the particles in this image belong to the first set. Area is the area of the particles in square inches. Major and Minor are the major and minor axes of the best fit ellipse in inches.

Area	Major	Minor
0.57011	1.21056	0.59963
0.11032	0.54541	0.25754
0.31244	0.79292	0.50171
0.10878	0.43522	0.31823
0.05323	0.30848	0.21971
0.52460	1.05428	0.63355
0.04320	0.31671	0.17368
0.25844	0.79024	0.41640
0.40733	0.82862	0.62590
0.16046	0.55249	0.36980
1.43029	1.56427	1.19119
0.60791	1.06871	0.73069
0.19055	0.56092	0.43954
0.30550	0.88784	0.44585
0.07252	0.39739	0.23235
0.12189	0.49065	0.31631
0.05400	0.32255	0.21317
0.06326	0.39266	0.20513
0.07715	0.37259	0.26363
0.73058	1.62431	0.57630
0.02546	0.19551	0.16580
0.08795	0.36457	0.30715
0.74292	1.12196	0.85185
1.95257	2.63240	0.94666
0.15738	0.51465	0.38935
0.53771	1.24446	0.55330
0.32787	0.81365	0.51307
0.30241	0.74565	0.52034
0.10029	0.53055	0.24068
0.01697	0.33558	0.06439
0.02932	0.26166	0.14265
0.22141	0.67816	0.41715
0.01852	0.27362	0.08616
0.06557	0.39393	0.21195
0.09489	0.52060	0.23207
0.05632	0.34392	0.20849

0.04397	0.31759	0.17629
0.41350	0.83499	0.63053
0.10800	0.42601	0.32280
0.04320	0.27857	0.19746
0.05169	0.29929	0.21989
0.04937	0.28341	0.22181
0.04783	0.30165	0.20189
3.42915	2.66577	1.64080
0.08023	0.34754	0.30525
0.20830	0.64798	0.40929
0.10569	0.51082	0.26344
0.10338	0.56847	0.23154
0.09026	0.53494	0.21484
0.31476	0.74685	0.53660
0.13655	0.51679	0.33642
0.02083	0.22012	0.12048
0.33790	0.79128	0.54372
1.40638	1.65568	1.08152
0.21987	0.71419	0.40022
0.92884	1.48991	0.79377
0.00771	0.15915	0.06172
0.21138	0.77278	0.34827
0.09720	0.44848	0.27596
0.04474	0.33236	0.17141
0.25844	0.79479	0.41402
0.05940	0.36713	0.20601
0.12266	0.63895	0.24443
0.05246	0.36049	0.18529
0.10955	0.68530	0.20353
0.04089	0.32892	0.15827
0.18438	0.80260	0.29250
0.10569	0.40861	0.32933
0.32170	0.81415	0.50310
0.33327	0.85481	0.49641
0.02237	0.24329	0.11709
0.22990	0.82897	0.36496
0.02083	0.22879	0.11592
0.19672	0.72928	0.34346
0.22835	0.59057	0.49231
0.24764	0.72038	0.43769
0.04397	0.26643	0.21014
0.22835	0.64245	0.45256
0.33096	0.80030	0.52654
0.29624	0.75413	0.50147
0.06017	0.36481	0.21001
0.03163	0.26042	0.15464
0.05092	0.30971	0.20932
0.13038	0.54044	0.30716
0.08718	0.41853	0.26520
0.06557	0.52943	0.15770
0.20907	0.86070	0.30927

0.03780	0.24337	0.19777
0.09026	0.52021	0.22092
0.36490	1.21574	0.38216
0.03317	0.24700	0.17100
0.02854	0.24178	0.15032
0.14118	0.50622	0.35509
0.09335	0.50353	0.23604
0.35256	0.99286	0.45608
0.07252	0.38774	0.23813
0.29624	0.69337	0.54399
0.05555	0.34954	0.21638
0.31399	0.76991	0.51926
1.09085	1.50070	0.93140
0.03009	0.22797	0.16804
0.15198	0.66067	0.29289
0.05786	0.35177	0.20943
0.03626	0.33878	0.13627
0.02314	0.29668	0.09932
0.28236	0.79558	0.45188
0.02546	0.30595	0.10595
0.03703	0.27181	0.17346
0.08178	0.35602	0.29245
1.09471	1.80711	0.77239
0.21061	0.67786	0.39559
0.06557	0.35755	0.23351
0.06095	0.37268	0.20821
0.11726	0.42871	0.34826
0.31476	1.04847	0.38223
0.05246	0.35776	0.18670
0.71438	1.27424	0.71459
0.26538	0.75066	0.45013
0.49374	0.99913	0.62919
0.03549	0.27106	0.16669
0.20212	0.67513	0.38119
0.04012	0.25729	0.19852
0.07483	0.37859	0.25167
0.03549	0.22910	0.19722
0.08332	0.40590	0.26135
0.03780	0.33695	0.14284
0.03934	0.41651	0.12027
0.18824	0.99229	0.24153
0.18901	0.54049	0.44525
0.13038	0.47085	0.35256
0.05015	0.39548	0.16144
0.15738	0.51720	0.38744
0.14118	0.68705	0.26163
0.05863	0.28603	0.26099
0.61794	0.99055	0.79429
0.00771	0.10872	0.09034
0.03163	0.23631	0.17042
0.12498	0.53283	0.29864

0.17358	0.69071	0.32140
0.13886	0.49171	0.35957
0.69509	1.22574	0.72202
0.40888	1.24498	0.42210
0.03857	0.30075	0.16330
0.09103	0.39326	0.29473
0.05246	0.30470	0.21921
0.69277	1.06126	0.83115
0.01852	0.27355	0.08618
0.05632	0.36055	0.19888
0.54697	1.31001	0.53162
0.09026	0.53620	0.21433
0.11418	0.45091	0.32240
0.11649	0.49654	0.29871
0.73212	1.08429	0.86514
0.21215	0.70248	0.38452
0.37570	0.81090	0.58991
0.30704	0.65983	0.59248
0.10878	0.44525	0.31106
0.34407	0.83839	0.52253
0.21061	0.62846	0.43294
0.03240	0.27512	0.14995
0.30010	0.67538	0.56575
0.08100	0.49434	0.20864
0.29933	0.78207	0.48732
0.41890	0.91768	0.58121
0.04937	0.30457	0.20640
0.09952	0.43508	0.29123
0.11418	0.42259	0.34401
0.05863	0.35151	0.21237
0.28853	0.97726	0.37591
0.96433	1.62299	0.76318
0.12035	0.64111	0.23901
0.36799	0.85016	0.55111
0.27156	0.71138	0.48604
0.48756	0.85561	0.72669
0.09412	0.41551	0.28841
0.09026	0.41159	0.27922
0.03472	0.26256	0.16835
0.03163	0.24416	0.16494
0.07869	0.59835	0.16744
0.14812	0.53041	0.35556
0.65497	1.36020	0.61598
0.10338	0.55530	0.23703
0.24841	0.60309	0.52444
0.03780	0.27621	0.17425
0.93424	1.34297	0.89963
0.20752	0.58941	0.44829
0.27850	0.76795	0.46174
0.17898	0.54490	0.41821
0.04474	0.42398	0.13437

0.28467	0.73750	0.49146
0.27773	0.80743	0.43795
0.28698	0.62927	0.58068
0.21832	0.78463	0.35428
0.07329	0.37985	0.24566
0.07175	0.37241	0.24529
0.45902	1.13235	0.51613
0.19055	0.68126	0.36334
0.04629	0.30679	0.19211
0.45439	1.21288	0.47862
0.17126	0.54199	0.40233
0.05940	0.47418	0.15950
1.38246	1.78672	0.98736
0.39499	1.10363	0.45569
0.26924	0.74763	0.45852
0.37339	0.86749	0.54803
0.13192	0.75058	0.22378
0.22835	0.91842	0.31657
5.72349	3.26896	2.22926
0.08178	0.33613	0.30976
0.09489	0.49835	0.24244
0.20367	0.74641	0.34873
0.43973	0.90725	0.61712
0.00771	0.12681	0.07746
0.08100	0.59001	0.17481
0.02237	0.30410	0.09367
0.31321	0.69469	0.57548
0.12266	0.44007	0.35489
1.05150	1.62165	0.82680
1.13019	1.47814	0.97353
0.76992	1.13017	0.86738
0.01234	0.20264	0.07756
0.27310	0.79189	0.43910
0.10183	0.44318	0.29257
0.31013	0.73343	0.53838
0.18747	0.63785	0.37421
0.08640	0.60039	0.18324
0.27618	0.98953	0.35537
0.04474	0.32072	0.18682
0.21370	0.80453	0.33819
0.10260	0.50226	0.26011
0.45131	0.79275	0.72484
0.28158	0.82855	0.43271
0.56857	0.92958	0.77877
0.04937	0.32822	0.19153
0.07175	0.43836	0.20839
0.03472	0.30157	0.14657
0.28004	0.84522	0.42185
0.21138	0.67537	0.39851
0.32170	0.77333	0.52966
0.03780	0.24408	0.19719

0.16278	0.66242	0.31288
0.04860	0.37780	0.16380
0.38496	0.84707	0.57864
0.54311	1.06266	0.65258
0.03394	0.31317	0.13801
0.53154	0.96199	0.71168
0.03780	0.25711	0.18720
0.20367	0.65010	0.39889
0.16355	0.70123	0.29696
0.54465	1.14702	0.60459
0.83781	1.62921	0.66199
0.22372	0.58673	0.48550
1.07156	2.08091	0.65565
0.09180	0.45203	0.25858
0.09103	0.52872	0.21922
0.19749	0.75087	0.33489
0.28236	0.63041	0.57027
0.33173	0.88756	0.47588
0.33250	1.13243	0.37384
0.38959	1.10327	0.44961
0.04937	0.31502	0.19956
0.17435	0.54693	0.40588
0.07483	0.46668	0.20416
3.19926	2.76990	1.47060
0.45131	1.01246	0.56755
0.04552	0.29560	0.19605
0.60637	1.03693	0.74456
0.01234	0.16621	0.09456
0.06403	0.32406	0.25158
0.13423	0.43285	0.39486
0.13115	0.54106	0.30862
0.07097	0.37484	0.24109
0.03086	0.20848	0.18846
0.29856	0.86155	0.44578
0.15969	0.50745	0.40068
0.25921	0.76181	0.43323
0.25613	0.70120	0.47068
0.11958	0.65808	0.23135
0.22372	0.82676	0.34455
0.08023	0.46817	0.21820
0.04552	0.29812	0.19440
0.55777	1.17384	0.60500
0.39113	0.83261	0.59813
0.09258	0.54219	0.21740
1.63859	1.87065	1.11529
0.15584	0.60941	0.32559
0.04089	0.28240	0.18435
0.30319	0.74311	0.51947
0.07792	0.34036	0.29148
0.41350	1.23512	0.42706
0.03317	0.21686	0.19477

0.03086	0.26500	0.14827
0.30396	1.03491	0.37395
0.18207	0.57873	0.40055
0.29778	0.81974	0.46253
0.04089	0.31397	0.16581
0.74446	1.19892	0.79061
0.05555	0.30811	0.22954
0.91958	1.59774	0.73282
0.03394	0.24442	0.17682
0.07175	0.32169	0.28397
0.11881	0.54157	0.27931
0.02700	0.24611	0.13969
0.06712	0.36746	0.23256
0.03009	0.27169	0.14100
0.02777	0.30361	0.11647
0.19827	0.53179	0.47470
0.41890	0.91145	0.58518
0.05940	0.30030	0.25186
0.45671	1.05306	0.55220
0.00771	0.12832	0.07655
0.08563	0.41651	0.26177
0.12883	0.49151	0.33374
0.19132	0.64952	0.37505
0.15815	0.46457	0.43343
0.14966	0.52631	0.36206
0.46751	0.99365	0.59905
0.94041	1.50146	0.79747
0.65343	1.35234	0.61521
0.12883	0.45049	0.36413
0.14041	0.49134	0.36384
0.17589	0.49647	0.45109
0.09643	0.56014	0.21920
0.07946	0.34463	0.29357
0.03086	0.26978	0.14564
0.46519	1.03226	0.57379
0.09798	0.43409	0.28737
0.25844	0.88603	0.37138
1.10551	1.48924	0.94516
0.45439	0.98100	0.59376
0.54388	0.95201	0.72740
0.04012	0.25805	0.19794
0.45516	0.95264	0.60834
0.03394	0.26546	0.16281
0.51379	0.92328	0.70855
0.25227	0.73994	0.43409
0.50994	0.89971	0.72164
0.05400	0.37592	0.18290
0.12883	0.51124	0.32086
0.11726	0.46117	0.32375
0.09412	0.47350	0.25308
0.32864	1.14516	0.36540

0.02392	0.22091	0.13784
0.20598	0.68942	0.38041
0.24455	0.71354	0.43638
0.15275	0.58506	0.33242
0.06712	0.37964	0.22510
0.17744	0.92535	0.24414
0.02469	0.28351	0.11087
0.03163	0.28143	0.14310
0.03472	0.31841	0.13882
0.03934	0.28392	0.17644
0.44976	0.83368	0.69044
0.24378	0.77493	0.40055
0.05169	0.41101	0.16012
0.07175	0.33201	0.27514
0.10183	0.47748	0.27155
0.27464	0.78327	0.44644
0.17126	0.54498	0.40013
0.14118	0.60069	0.29925
0.40425	1.04397	0.49302
0.03626	0.28837	0.16009
0.21910	0.75225	0.37083
0.67117	1.06719	0.80076
0.11032	0.39390	0.35659
0.16432	0.61876	0.33813
0.28853	0.74866	0.49069
0.07792	0.34942	0.28393
1.23203	1.55664	1.00773
0.03549	0.27631	0.16353
0.06249	0.41097	0.19360
1.25903	1.41417	1.13356
0.13115	0.52163	0.32012
0.11109	0.53025	0.26675
1.10319	1.36326	1.03971
0.43356	0.87663	0.62972
0.49991	1.21012	0.52598
0.19981	0.72383	0.35147
0.06095	0.37443	0.20724
0.20367	0.73736	0.35168
0.50608	1.18818	0.54231
0.04552	0.33113	0.17502
0.85015	1.61508	0.67021
0.21215	0.72093	0.37468
0.06095	0.28963	0.26792
0.05092	0.28400	0.22827
0.39730	0.80811	0.63084
0.04089	0.30685	0.16966
0.04089	0.29159	0.17854
0.09335	0.42273	0.28116
0.04706	0.30482	0.19656
0.05015	0.42535	0.15010
0.73289	1.28773	0.72464

0.06943	0.45222	0.19549
0.05400	0.35789	0.19212
1.09394	1.38721	1.00406
0.04166	0.26481	0.20030
0.07020	0.40483	0.22080
0.04629	0.38508	0.15305
0.10106	0.50699	0.25381
0.08332	0.41187	0.25756
7.40836	3.74375	2.51956
0.09412	0.40657	0.29475
1.35700	1.66962	1.03484
0.92113	1.47556	0.79483
0.25227	0.73265	0.43841
0.04474	0.40178	0.14180
0.22372	0.81621	0.34900
0.06712	0.42315	0.20195
0.22527	0.64639	0.44373
0.05246	0.31471	0.21224
0.18207	0.50305	0.46081
0.05709	0.38372	0.18943
2.69704	2.11787	1.62143
0.19672	0.70495	0.35531
0.04397	0.31908	0.17547
0.52228	1.23877	0.53681
0.04012	0.32757	0.15593
0.41890	0.96901	0.55043
0.66423	2.06337	0.41083
0.31167	0.67926	0.58421
0.18515	1.25902	0.18724
0.84861	1.33936	0.80745
0.91804	1.25045	0.93477
0.40733	0.99174	0.52295
0.27156	0.85461	0.40457
0.04012	0.34506	0.14802
0.03086	0.22398	0.17542
0.08100	0.37671	0.27378
0.14966	0.44441	0.42879
0.04012	0.23877	0.21392
0.07637	0.37016	0.26271
0.05092	0.30275	0.21413
0.25613	0.64378	0.50656
0.04089	0.26675	0.19516
1.65710	1.56689	1.34654
0.03240	0.27338	0.15090
0.50531	1.13395	0.56738
0.23298	0.80076	0.37045
0.12035	0.52108	0.29407
0.44976	0.90093	0.63563
0.01543	0.18202	0.10793
0.11263	0.45496	0.31521
1.20734	1.32020	1.16439

0.48525	1.04432	0.59162
0.08332	0.42411	0.25014
0.09720	0.65792	0.18811
1.03993	1.44533	0.91611
0.20444	0.73289	0.35517
0.20367	0.57978	0.44727
0.77995	1.32744	0.76512
0.31167	0.91130	0.43546
0.08640	0.60040	0.18323
0.06095	0.61536	0.12610
0.09875	0.52796	0.23814
0.28853	0.79878	0.45990
0.35796	1.12965	0.40346
0.15044	0.65749	0.29132
0.08718	0.71027	0.15627
0.10415	0.44631	0.29712
0.16201	0.58955	0.34988
0.02006	0.25176	0.10144
0.37725	1.01644	0.47255
0.29316	0.66424	0.56193
0.51765	1.02553	0.65131
0.39345	1.30177	0.38482
0.58708	1.19988	0.62298
0.02237	0.25987	0.10961
0.10106	0.40028	0.32147
0.16741	0.69903	0.30492
0.49837	1.09415	0.57994
0.03857	0.25036	0.19617
0.02469	0.22815	0.13777
0.54388	1.25873	0.55015
0.06943	0.34814	0.25393
0.33636	0.76456	0.56014
2.93542	2.46209	1.51802
0.34793	1.04090	0.42559
0.21370	0.62729	0.43375
0.16895	0.65065	0.33062
2.88527	3.02168	1.21576
0.32401	0.73812	0.55892
0.26538	0.78087	0.43272
0.71206	1.28091	0.70779
0.31321	0.71625	0.55679
0.20598	0.81058	0.32355
1.18805	1.91032	0.79184
0.05940	0.32861	0.23017
0.55623	1.02675	0.68976
0.14966	0.52605	0.36224
1.41564	2.42202	0.74500
0.05786	0.40029	0.18404
0.01697	0.18335	0.11786
0.59094	1.46082	0.51506
0.46519	1.04406	0.56730

0.33790	0.91368	0.47088
0.07020	0.43990	0.20319
0.77301	1.47391	0.66776
0.36645	0.87496	0.53325
0.07715	0.58056	0.16919
0.60251	1.14613	0.66934
0.35102	0.77183	0.57905
0.44668	0.91348	0.62259
0.10183	0.54800	0.23660
0.33713	1.00061	0.42899
0.24455	0.80516	0.38672
0.26307	0.93545	0.35806
0.03317	0.26475	0.15954
0.20289	1.15480	0.22370
0.04706	0.41684	0.14374
0.10878	0.83921	0.16503

APPENDIX C

DATA FOR CALCULATION OF COEFFICIENT OF VARIATION

Following is the data used to calculate the coefficient of variation for various bin sizes for zoomed(6 images) and unzoomed(10 images) images.

Mid Point of the bin	Mean - unzoomed	Standard Deviation	Coeff. of Variation	Mean - zoomed	Standard Deviation	Coeff. of Variation
0.25	0.082	0.0493	0.6014	0.4722	0.1461	0.3095
0.75	0.2193	0.0293	0.1338	0.1673	0.0549	0.3279
1.25	0.1751	0.0301	0.1719	0.1526	0.0573	0.3759
1.75	0.1368	0.0292	0.2135	0.0906	0.0458	0.5051
2.25	0.1153	0.0236	0.2046	0.0515	0.0278	0.5388
2.75	0.2716	0.0614	0.2261	0.0658	0.0371	0.5633

REFERENCES

Aimone, C. T., and Dowding, C. H. 1983. Fragmentation Measurement Results for Fourteen Full-Scale Production Blasts: A Comparison with a Three Dimensional Wave Code. Proceedings of the 9th Conference on Explosives and Blasting Technique: 310-333.

Ballard, D. H., and Brown, C. M. 1982. Computer Vision, Prentice Hall, NJ, 523 pages.

Bhandari, S., and Vutukuri, V. S. 1974. Rock Fragmentation With Longitudinal Explosive Charges. Proceedings of the 3rd Congress of the ISRM 2B: 1337-1342.

Bowie, J. E., and Young, I. T. 1977. An Analysis technique for biological shape -- 2, Acta Cytologica 21: 455-464.

Carter, J.W. 1977. Analysis of a Simple Photographic Method Proposed for Determining Size Distribution of Ore Fragments. USBM Lab Report RBM 77-03 : 1-19.

Chassery, J. M., and Gaybay, C. 1984. An iterative segmentation method based on a contextual color and shape criterion, IEEE Transactions PAMI-6: 794-800.

Clark, G. B. 1987. Principles of Rock Fragmentation, John Wiley and Sons, NY, 606 pages.

Dick, R.A., Fletcher, L.A., and D'Andrea, D.V. 1973. A Study of Fragmentation from Bench Blasting at a Reduced Scale. USBM Report 7704 : 1-22.

Farmer, I. W., Kemeny, J. M., and McDoniel, C. 1991. Analysis of Rock Fragmentation in Bench Blasting Using Digital Image Processing. Proceedings of the 7th International Congress on Rock Mechanics, Aachen, Germany: 1037-1042.

Frankenburg, A. C. 1990. The application of image processing to the analysis of particle size and shape in loose sediments. University of North Carolina, United States: Doctoral Thesis.

Franklin, J. A., and Maerz, N. H. 1986. Digital Photo-Analysis of Rock Jointing. 39th Canadian Geotechnical Conference: 11-20.

Franklin, J. A., and Maerz, N. H., and Bennett, C. P. 1988. Rock mass characterization using photonalysis, International Journal of Mining and Geological Engineering, 6: 97-112.

Gama, C. D. 1984. Microcomputer Simulation of Rock Blasting to Predict Fragmentation. Proceedings of the 25th U.S. Symposium on Rock Mechanics: 1018-1030.

Gaybay, C. 1986. Image structure representation and processing: a discussion of some segmentation methods in cytology, IEEE Transactions PAMI-8, 140-146.

Ghosh, A., Daemen, J. J. K., and van Zyl, D. 1990. Fractal based approach to determine the effect of discontinuities on blast fragmentation. Proceedings of the 31st U.S. Rock Mechanics Symposium, Golden, CO.

Gonzalez, R. C., and Wintz, P. 1987. Digital Image Processing, 2nd Ed., Addison Wesley, 503 pages.

Gozon, J. S., Britton, R. R., and Fodo, J. D. 1986. Predetermining Average Fragment Size: A Case Study. International Symposium on Application of Rock Characterization Techniques in Mine Design: 190-195.

Greenland, B. J., and Knowles, J. D. 1969. Rock Breakage. Mining Magazine 120: 76-83.

Hunter, G.C., McDermott, C., Miles, N.J., Singh, A., Scoble, M.J. 1990. Review of Image Analysis Techniques for Measuring Blast Fragmentation. Mining Science & Technology v 11(1) : 19-36.

Ji, Liang 1989. Intelligent splitting in the chromosome domain. Pattern Recognition, 13: 519-532.

Just, G. D., and Henderson, D. S. 1971. Model Studies of Fragmentation of Explosives. Proceedings of the 1st Australia-New Zealand Conference on Geomechanics 1: 238-245.

Lovely, B. G. 1973. A Study of the Sizing Analysis of Rock Particles Fragmented by a Small Explosive Blast. Australian Geomechanics Society National Symposium on Rock Fragmentation, Adelaide: 24-34.

MacKenzie, A. S. 1966. Cost of Explosives - Do You Evaluate it Properly? Mining Congress Journal, May 1966: 32-41.

Maerz, N. H., Franklin, J. A., Rothenburg, L., and Coursen, D. 1987. Measurement of rock fragmentation by digital photoanalysis. Proceedings of the Congress of the International Society for Rock Mechanics, 6 (1): 687-692.

Mojtabai, N., Cetinas, A., Farmer, I. W., and Savely J. P. 1989. In-place and excavated block size distribution. Proceedings of the 30th Rock Mechanics Symposium, Morgantown, WV: 537-543.

Noren, C. H., and Porter, D. D. 1974. A comparison of Theoretical Explosive Energy and Energy Measured Underwater with Measured Rock Fragmentation. Proceedings of the 3rd Congress of the ISRM 2B: 1371-1375.

Ord, A. 1989. Real time image analysis of size and shape distribution of rock fragments. The AusIMM Bulletin and Proceedings, 294(1): 28-31.

Singh, D. P., Appa Rao, Y.V., and Saluja, S. S. 1980. A Laboratory Study of Effects of Joints on Rock Fragmentation. Proceedings of the 21st U.S. Symposium on Rock Mechanics: 400-410.

Vanderheydt, L., and Dom, F. 1981. Two-dimensional shape decomposition using Fuzzy Subset Theory applied to automated chromosome analysis. Pattern Recognition, 13: 147-157.

Wu, X., and Kemeny, J.M. In press. Computer Delineation of Rock Fragments in Photographic Images of Blasted Rock.

Young, T. Y., and Fu, K.-S. 1986. Handbook of Pattern Recognition and Image Processing, Academic Press, San Diego, 705 pages.